

AD-A243 697

AFIT/GE/ENG/91D-24

DEC 17 1991

DETERMINATION OF BISTATIC RADAR CLUTTER POWER FROM
TOPOGRAPHIC DATA

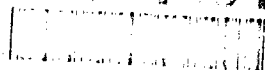
THESIS

Clyde Richard Heddings
Captain, USAF

AFIT/GE/ENG/91D-24

Approved for public release; distribution unlimited

91-10075



91 12 24 003

20000901001

| REPORT DOCUMENTATION PAGE | | | Form Approved OMB No. 0704-0188 | |
|--|--|--|--------------------------------------|--|
| <small>Public reporting burden for this collection of information is estimated to average 1 hour per response, including the time for reviewing instructions, searching existing data sources, gathering and maintaining the data needed, and completing and reviewing the collection of information. Send comments regarding this burden estimate or any other aspect of this collection of information, including suggestions for reducing this burden, to Washington Headquarters Services, Directorate for Information Operations and Reports, 1215 Jefferson Davis Highway, Suite 1204, Arlington, VA 22202-4302 and to the Office of Management and Budget, Paperwork Reduction Project (0704-0188), Washington, DC 20503.</small> | | | | |
| 1. AGENCY USE ONLY (Leave blank) | 2. REPORT DATE Dec 91 | 3. REPORT TYPE AND DATES COVERED Master's Thesis | | |
| 4. TITLE AND SUBTITLE Determination of Bistatic Radar Clutter Power From Topographic Data | | 5. FUNDING NUMBERS | | |
| 6. AUTHOR(S) Clyde R. Heddings, Capt, USAF | | | | |
| 7. PERFORMING ORGANIZATION NAME(S) AND ADDRESS(ES) Air Force Institute of Technology, WPAFB OH 45433-6583 | | 8. PERFORMING ORGANIZATION REPORT NUMBER AFIT/GE/ENG/91D-24 | | |
| 9. SPONSORING/MONITORING AGENCY NAME(S) AND ADDRESS(ES) | | 10. SPONSORING/MONITORING AGENCY REPORT NUMBER | | |
| 11. SUPPLEMENTARY NOTES | | | | |
| 12a. DISTRIBUTION/AVAILABILITY STATEMENT Approved for public release; Distribution unlimited. | | 12b. DISTRIBUTION CODE | | |
| 13. ABSTRACT (Maximum 200 words) The purpose of this research was to develop a procedure for estimating the average bistatic radar clutter power from a topographic map and using rough surface scattering theory. First, the terrain in the radar target area was divided into sub regions having homogeneous characteristics. A joint Gaussian distribution for the surface heights was fitted from the information contained in the topographic map contour lines for each homogeneous area. From these distributions, the normalized radar cross section for each terrain area was determined. The clutter power for each range cell was then determined via a modified radar range equation. The procedure was implemented for three target areas of an existing ground based bistatic system near Hanscom AFB, MA using a U. S. Geological Service topographic map of the area. Scattered power from very rough surfaces was estimated. However, the accuracy of the estimates could not be verified due to a lack of actual data for comparison. It was also determined that topographic map data may not be sufficient to determine scattered power from slightly rough surfaces. | | | | |
| 14. SUBJECT TERMS Radar, Ground based radar, Bistatic radar, Clutter, Radar scattering, Electromagnetic scattering | | 15. NUMBER OF PAGES 115 | | |
| | | 16. PRICE CODE | | |
| 17. SECURITY CLASSIFICATION OF REPORT Unclassified | 18. SECURITY CLASSIFICATION OF THIS PAGE Unclassified | 19. SECURITY CLASSIFICATION OF ABSTRACT Unclassified | 20. LIMITATION OF ABSTRACT UL | |

REPRODUCTION QUALITY NOTICE

This document is the best quality available. The copy furnished to DTIC contained pages that may have the following quality problems:

- **Pages smaller or larger than normal.**
- **Pages with background color or light colored printing.**
- **Pages with small type or poor printing; and or**
- **Pages with continuous tone material or color photographs.**

Due to various output media available these conditions may or may not cause poor legibility in the microfiche or hardcopy output you receive.

☐ **If this block is checked, the copy furnished to DTIC contained pages with color printing, that when reproduced in Black and White, may change detail of the original copy.**

AFIT/GE/ENG/91D-24

DETERMINATION OF BISTATIC RADAR CLUTTER POWER
FROM TOPOGRAPHIC DATA

THESIS

Presented to the Faculty of the School of Engineering
of the Air Force Institute of Technology

Air University

In Partial Fulfillment of the
Requirements for the Degree of
Master of Science in Electrical Engineering

Clyde Richard Heddings, B.S.E.
Captain, USAF

December 1991

| | |
|--------------------|----------------------|
| Accession For | |
| NTIS | SI |
| DTIC | SI |
| Unannounced | SI |
| Justification | |
| By | |
| Distribution/ | |
| Availability Codes | |
| Dist | Avail and/or Special |
| A-1 | |



Approved for public release; distribution unlimited

Preface

This research is intended to provide a practical and easily understood approach using rough surface scattering theory to estimate the clutter power intercepted by a ground based bistatic radar system. The procedure obtains estimates of normalized radar cross section for homogeneous sections of terrain based upon the statistical properties of the terrain heights. From a knowledge of the antenna beam widths and location of the isorange contour lines associated with the bistatic system, the normalized radar cross sections can be used to determine the clutter power for each radar range cell from a modified radar range equation.

I would like to acknowledge all the assistance provided to me during the course of this project by my advisor, Dr. Vital Pyati. Special thanks also goes to Lt Col David E. Meer for providing me with a basic education in the area of radar fundamentals and for providing me with an occasional nudge in the right direction. Many thanks also go to the sponsor of the project, Dr. K. V. N. Rao and his associate Mr. John Lennon from RADC/EECE. Both of these gentlemen provided much needed insight for the completion of this project.

On a personal note, I would like to thank Captain Mike Temple for all the personal and professional guidance he has bestowed upon me throughout my stay at AFIT. I don't know if I would have made it without your help

Finally, I especially want to thank my family for all of their support and understanding during the past eighteen months. To my wife Debbie, thanks for remaining my best friend throughout the ordeal that is associated with a tour at AFIT. To my children Andrea and Grant, your patience with me during these times will never be forgotten.

Clyde Richard Heddings

Table of Contents

| | Page |
|--|------|
| Preface | ii |
| Table of Contents | iii |
| List of Figures | v |
| List of Tables | vi |
| Abstract | vii |
| I Introduction | 1-1 |
| 1.1 Background. | 1-1 |
| 1.2 Problem Statement. | 1-4 |
| 1.3 Research Objective. | 1-4 |
| 1.4 The Bistatic System. | 1-4 |
| 1.5 Assumptions. | 1-5 |
| 1.6 Scope. | 1-6 |
| 1.7 Approach. | 1-7 |
| 1.7.1 Radar Antenna Footprints. | 1-7 |
| 1.7.2 Terrain Maps. | 1-7 |
| 1.7.3 Clutter-to-Noise Power Profile Maps. | 1-9 |
| 1.7.4 Performance Evaluation. | 1-10 |
| 1.8 Overview of the Thesis. | 1-10 |

| | Page |
|--|------|
| II. Theory | 2-1 |
| 2.1 Overview. | 2-1 |
| 2.2 Clutter-To-Noise Power Ratio. | 2-1 |
| 2.2.1 Factors Affecting the Clutter Power. | 2-2 |
| 2.3 Determining the Antenna Footprint. | 2-4 |
| 2.3.1 The Equirange Contour Lines. | 2-4 |
| 2.3.2 The Antenna Patterns. | 2-14 |
| 2.4 Determining the Incoherent Contribution Power. | 2-16 |
| 2.4.1 Rough Surface Models. | 2-16 |
| 2.4.2 Incoherent Scattering From a Slightly Rough Surface. | 2-18 |
| 2.4.3 Incoherent Scattering From Very Rough Surfaces | 2-20 |
| III. Application of the Process and Results | 3-1 |
| 3.1 Known System Parameters. | 3-1 |
| 3.2 Establishing the Clutter Cells. | 3-2 |
| 3.2.1 Identifying the Equirange Contour Lines. | 3-2 |
| 3.2.2 Identifying the Antenna Patterns. | 3-2 |
| 3.2.3 Identifying the Clutter Cells. | 3-10 |
| 3.3 Terrain Site Characterization. | 3-13 |
| 3.3.1 Determining the Sample Point Mean Value. | 3-17 |
| 3.3.2 Determining the Sample Point Variance. | 3-18 |
| 3.3.3 Estimating the Sample Mean and Variance. | 3-19 |
| 3.3.4 Estimating the Sample Correlation Length. | 3-20 |
| 3.4 Determining the NRCS of the Site Characterization Block. | 3-22 |
| 3.5 Calculating the Range Cell Power. | 3-23 |
| 3.5.1 Clutter Power for Site One. | 3-26 |
| 3.5.2 Clutter Power for Site Two. | 3-32 |
| 3.5.3 Clutter Power for Site Three. | 3-32 |

| | Page |
|---|--------|
| IV. Conclusions and Recommendations | 4-1 |
| 4.1 Conclusions | 4-1 |
| 4.2 Recommendations | 4-3 |
| Appendix A. Software | A-1 |
| Appendix B. Topographic Data | B-1 |
| Bibliography | BIB-1 |
| Vita | VITA-1 |

List of Figures

| Figure | Page |
|--|------|
| 2.1. Bistatic scattering geometry. | 2-3 |
| 2.2. Two dimensional bistatic geometry. | 2-5 |
| 2.3. Ground based bistatic system timing diagram. | 2-6 |
| 2.4. Relationship between slant ranges and xy-plane distances. | 2-7 |
| 2.5. equirange contour lines for a ground based bistatic system. | 2-9 |
| 2.6. Basic geometry for an ellipse. | 2-10 |
| 2.7. Geometry for the case when $R_T = R_R$ | 2-11 |
| 2.8. Clutter Blocks Created by the Antenna Patterns. | 2-14 |
| 3.1. Pyramidal Horn Geometry. | 3-8 |
| 3.2. Terrain Scattering Geometry. | 3-14 |
| 3.3. Terrain Site Characterization Geometry. | 3-16 |
| 3.4. Determining the Sample Point Mean from Contour Lines. | 3-17 |

List of Tables

| Table | Page |
|---|------|
| 3.1. Site Characterization Data. | 3-24 |
| 3.2. NRCS Data from <i>Sigma</i> .for. | 3-25 |
| 3.3. Site One Area and Range Data for Vertical Polarization. | 3-28 |
| 3.4. Site One Clutter Block Power, Vertical Polarization. | 3-29 |
| 3.5. Site One Area and Range Data for Horizontal Polarization. | 3-30 |
| 3.6. Site One Clutter Block Power, Horizontal Polarization. | 3-31 |
| 3.7. Site Two Area and Range Data for Vertical Polarization. | 3-33 |
| 3.8. Site Two Clutter Block Power, Vertical Polarization. | 3-34 |
| 3.9. Site Two Area and Range Data for Horizontal Polarization. | 3-35 |
| 3.10. Site Two Clutter Block Power, Horizontal Polarization. | 3-36 |
| 3.11. Site Three Area and Range Data for Vertical Polarization. | 3-37 |
| 3.12. Site Three Area and Range Data for Horizontal Polarization. | 3-38 |

Abstract

The purpose of this research was to develop a procedure for estimating the average bistatic radar clutter power from a topographic map and using rough surface scattering theory. First, the terrain in the radar target area was divided into sub regions having nearly homogeneous characteristics. A joint Gaussian distribution for the surface heights was fitted from the information contained in the topographic map contour lines for each homogeneous area. From these distributions, the normalized radar cross section for each terrain area was determined. The clutter power for each range cell was then determined via a modified radar range equation.

The procedure was implemented for three target areas of an existing ground based bistatic system near Hanscom AFB, Massachusetts using a U. S. Geological Service topographic map of the area. Scattered power from very rough surfaces was estimated. However, the accuracy of the estimates could not be verified due to a lack of actual data for comparison. It was also determined that topographic map data may not be sufficient to determine scattered power from slightly rough surfaces.

DETERMINATION OF BISTATIC RADAR CLUTTER POWER FROM TOPOGRAPHIC DATA

I. Introduction

1.1 Background.

The operating principles of radar are relatively simple. The process initiates when a transmitter emits an identifiable electromagnetic wave into the atmosphere. When the wave strikes an object, electromagnetic energy scatters in all directions. A receiver detects the presence of a target when the reflected energy strikes the receive antenna. Given knowledge of the exact time of transmission of the original wave and of the velocity of wave propagation, the receiver can calculate the approximate range between the target and the radar system. If the energy from the transmitter is concentrated in a narrow beam, the bearing and elevation of the target can also be determined. With these capabilities, it is easy to see how radar has evolved into a necessary piece of military hardware. It finds application on every military aircraft in the inventory today and its capabilities often play a vital role in the success or failure of a mission.

Problems arise when the reflected energy is not due solely from a desired target. When the transmitting antenna directs energy at low grazing angles, objects on the ground reflect energy to the receiver. This phenomenon is known as clutter. The amount of clutter energy returned to the radar receiver is proportional to the reflectivity of the terrain and other factors. When more energy is reflected from terrain features than from a desired target the capabilities of a radar are reduced.

All military forces attempt to use clutter to their advantage. Low flying aircraft and missiles are difficult to detect in the presence of clutter. The clutter energy obscures target reflections and provides an attacking force with the advantage of less time of exposure to hostile countermeasures. The detection of low flying objects is compounded by the use of stealth technology, which reduces the amount of energy reflected in the backscatter direction. Monostatic radar systems use collocated transmitters and receivers. The transmitter and receiver often share a common antenna and the system only detects backscattered target energy. With less electromagnetic energy reflected toward a receiver by using stealth technology, the task of hiding an incoming vehicle in ground clutter becomes easier.

This work is sponsored by the Applied Electromagnetics Division of the Rome Air Development Center (RADC). RADC has proposed using bistatic radar systems with special configurations as a technique to enhance the detection of low observable (stealthy) objects. Bistatic radar systems use transmitters and receivers which are not collocated (18:1) and do not rely on backscattered energy for proper operation.

RADC proposes that, for a given terrain and bistatic angle, there will be a transmitter to receiver antenna polarization relation which will result in a minimum amount of clutter return from the terrain in question. Use of the process to enhance the detection of low observable objects requires apriori knowledge of the required antenna polarization relationship which is obtained from the reflective characteristics of the terrain. To obtain optimum performance of the bistatic configuration proposed by RADC, a thorough knowledge of the clutter-to-noise power profiles of bistatic radars operating at low grazing angles is needed.

For the foregoing reasons there is considerable interest in predicting the terrain reflectivity seen by bistatic radar systems at low grazing angles. The clutter-to-noise power levels at a radar receiver antenna are directly related to the reflectivity of the terrain in the target area. Several analytical and empirical models (13:671-773), (9:74-134), (3:70-119) have been proposed to calculate the terrain reflectivity from known

topological features.

The amount of clutter power a bistatic radar detects depends on the radar parameters, the geometric locations of the transmitter, receiver, and target area as well as the physical characteristics of the terrain.

The radar parameters include the frequency of operation of the transmitter, the transmit and receive antenna polarizations, the transmit and receive antenna beamwidths, and the transmitter pulse width. All of these parameters are controllable by the radar design engineer.

The geometric considerations involve the physical locations of the transmitter and the receiver in relation to the target area. The most prominent of these factors are:

- The distance between the transmitter and receiver.
- The distance from the transmitter to the target area.
- The distance from the receiver to the target area.
- The bistatic angle formed by the transmitter, receiver, and target.
- The height of the transmitting and receiving antennas.
- The grazing angle of the transmitting and receiving antennas.

The physical characteristics of the terrain can not be controlled and must be measured or estimated for each particular application. The terrain factors which affect the amount of reflected clutter power are:

- The physical characteristics of the terrain.
 1. Flat land, rolling hills, mountains, bodies of water.
 2. The amount of moisture in the soil.
 3. The dielectric constant of the terrain.

- The population of the terrain.
 1. The specific type of vegetation, trees, or buildings covering the terrain.
 2. The relative heights, thicknesses, and densities of the population.
 3. The dielectric constants of the population items.
- The weather conditions in the target area.

All of these factors affect the amount of clutter power received by a bistatic radar system.

1.2 Problem Statement.

No accurate procedure exists for determining the clutter-to-noise power profile of a ground based bistatic radar system operating at low grazing angles and large Bistatic angles from knowledge of the terrain features of the radar target area.

1.3 Research Objective.

The purpose of this research effort is to develop an accurate procedure for predicting the clutter-to-noise power profile for a ground based bistatic radar system from knowledge of the target area topography.

1.4 The Bistatic System.

The transmitter for the bistatic radar system used for this thesis was an S band weather radar located near Stow, Massachusetts. The receiver was an RADC asset located atop Prospect Hill in Waltham, Massachusetts. The proposed target area was the terrain southwest of Hanscom Air Force Base. Stow is located approximately 20 kilometers (Km) west of Waltham. RADC originally requested clutter-to-noise power ratios for five range bins at three different bistatic angles between 120° and 160°. The clutter powers were to include the effects of the power associated with the

main lobes and significant side lobes of both antennas. The researcher was at liberty to select the appropriate bistatic angles and range bins. As the project progressed, three specific sites were selected by RADC.

The transmitter was operated at a frequency of 3 gigahertz (GHz), had a peak power of 800 kilowatts (KW), a pulse width of 1 microsecond (μs), and a pulse repetition frequency (PRF) of 1 kilohertz (KHz). The transmitting antenna was a 28 foot parabolic reflector and could be operated with vertical or horizontal polarization.

The range gated receiver was equipped with a 20 dB standard gain horn antenna and could operate with either vertical or horizontal polarization. The term *standard gain horn* was taken to mean a pyramidal horn antenna designed for optimum gain in both the E plane and H plane.

1.5 Assumptions.

The radar range cells were assumed to be in the far field of both the transmitting antenna and receiving antenna. This implied the wavefronts incident upon the terrain and the receiving antenna aperture were planar. This was a valid assumption given the geometry of the test area. Skolnik (15:229) describes the far field as a distance greater than R_F where R_F is defined as:

$$R_F = D^2/\lambda \quad (1.1)$$

Where:

D = the largest dimension of the antenna aperture in meters (m)

λ = the wavelength of the radar in meters

The wavelength, λ , was determined from (11:1)

$$\lambda = c/f \quad (1.2)$$

Where:

c = the velocity of wave propagation, $c = 3 \times 10^8$ meters/second (m/s)

f = the operating frequency of the radar in Hertz (Hz)

Using an operating frequency of 3.0 GHz in Eq 1.2 yielded $\lambda = 10$ centimeters (cm). The largest dimension of the receiver antenna aperture was 45 cm and the transmitter antenna had an diameter of 28 feet or 8.5344 m. Eq 1.1 was used to calculate R_F as 2.025 m for the receiver and 728.36 m for the transmitter. Since the range from either the transmitter or the receiver (20 Km) was much greater than R_F , the target area was in the far field and the planar wavefront assumption was valid.

The procedure developed during this research was limited to stationary ground based bistatic systems operating at low grazing angles and all bistatic angles except the forward scatter and back scatter directions. The radar receiver was assumed to be operating without using pulse integration.

1.6 Scope.

This thesis was limited to the development of a process for the determination of the clutter-to-noise power profile for a generic ground based bistatic system. The process was then applied to five range cells for three bistatic angles of the specific bistatic radar system used by RADC. The range cells selected for analysis represent only a small sample of the total target area. The clutter-to-noise power profile concept could easily be extended to an entire target area.

The effects on the clutter-to-noise power profiles of extreme weather conditions, variations in soil moisture content, and variations in target area population were not considered in this research effort.

1.7 Approach.

The research was accomplished in several steps. Barrick (13:671-729) details processes for calculating scattered power from two classes of rough surfaces. His description encompasses coherent and incoherent scattering from slightly rough surfaces and incoherent scattering from very rough surfaces. Both cases treat the height of the surface as a random variable and require knowledge of the distribution of the surface heights. Therefore each target site was subdivided and analyzed to obtain the necessary statistical information.

Topographic data for the selected target sites was digitized and entered in a data base. The data was analyzed to develop statistical representations of the terrain characteristics. Existing rough surface scattering procedures were used to predict the clutter-to-noise power profile of three range cells at each site. The process was initiated by determining the footprint of the bistatic radar.

1.7.1 Radar Antenna Footprints. The radar footprint is the terrain area delineated by the intersection of the projected transmit and receive antenna patterns and the concentric ellipses which define the isorange contours of a bistatic radar system. The size and shape of the individual range cells were determined by several factors:

1. The radiation patterns of both antennas.
2. The relative heights of the antennas and the target area.
3. The bistatic angle formed by the transmitter, receiver, and target area.
4. The distance from transmitter to target and receiver to target.
5. The range gating interval used in the receiver.

1.7.2 Terrain Maps. Topographic maps for the target area were obtained from the United States Geological Service (USGS) to correlate the physical characteristics of the terrain to the selected range cells. The maps were scaled to 1/250000

and allowed analysis of the ground cover in the area of interest. The three range cells selected for evaluation at each bistatic angle were subdivided into smaller blocks for statistical analysis to determine the mean, variance, and correlation length of the terrain height distributions covered by the selected range cells.

The information from the topographic maps for the specific blocks of each range cell was transferred to a memory array where the data was used to determine the large scale of roughness parameters. Specifically, the data represents the relative position (x - y coordinates), height, dielectric constant, and type of the terrain inhabiting the range cell blocks.

Though the USGS maps are detailed, they lack sufficient information to describe the range cell blocks completely. The maps provide detailed information on the locations and relative sizes of buildings, roads, streams, and major bodies of water. The elevation data is provided in the form of three meter contour lines and is accurate enough to determine the necessary large scale of roughness parameters required for the RADC application.

The land cover on the USGS maps was identified as falling into one of sixteen broad categories. Examples of these categories are woodland, scrub, marsh, swamp, mangrove, orchard, and vineyard. Though informative, the information was not detailed enough to determine the small scale of roughness parameters for the specific RADC application. If the entire range cell in question had a homogeneous population, e.g. all of the blocks in range cell one were entirely covered by pine trees, additional information would still be required. The additional information would have to be detailed enough to identify individual tree heights so that a height distribution could be developed. The mean and variance of the height distribution would then be used to calculate the incoherent power scattered by the small scale of roughness. Information is also needed to determine the relative permittivity of the target area surface and any vegetation which may inhabit surface.

Unfortunately nature is not this cooperative. It is unlikely that the entire

range cell will have a homogeneous small scale of roughness. The extreme case would involve a different small scale of roughness for each range cell block. In this instance a separate height distribution would have to be developed for each range cell block. This process could rapidly become computationally cumbersome if developing a clutter-to-noise power map for the entire coverage area of a specific bistatic radar system.

1.7.3 Clutter-to-Noise Power Profile Maps. To simplify the calculations required, areas of homogeneous surface characteristics were selected at each target area. The height distributions in these areas were assumed to be Gaussian in nature. The mean, variance, and correlation distance were extracted from the data available on the topographic maps. The characteristics of the identified Gaussian PDF were used to implement Barrick's rough surface scattering formulas.

Applying Barrick's formulas to each range cell characterization area provided a value for the normalized radar cross section (NRCS) of the block. The area of the selected range cells was used to determine an average value of RCS which in turn was used in a variation of the bistatic radar range equation to determine the scattered power at the receiver. In the cases where the terrain exhibits both scales of roughness over a single range cell, the scattered power for both cases could be calculated and added vectorially.

The implementation of the scattering formulas was essentially the same. The main difference in the two cases (slightly rough surfaces and very rough surfaces) was in how they were developed and their surface height variations relative to the wavelength of the excitation source. The very rough surface formulas were developed using physical optics principles. The slightly rough surface formulas were developed using a perturbation technique.

Plotting the values of clutter-to-noise power for each cell relative to the cell's physical position yields a clutter-to-noise power profile map for the bistatic radar.

The concept is easily extended to include the entire radar footprint.

1.7.4 Performance Evaluation. The results of this research were to be verified with the equipment already in place at the RADC bistatic radar sites. The actual data was unavailable at the time of publication.

1.8 Overview of the Thesis.

Chapter II presents the theory behind the procedures pertaining to the determination of clutter reflectivity. Chapter III presents the results of the research effort and Chapter IV presents conclusions from the thesis and makes recommendations for further research.

II. Theory

2.1 Overview.

This chapter describes the procedures used to calculate the clutter-to-noise power ratios for each range bin and provides the theory behind the concepts employed here.

2.2 Clutter-To-Noise Power Ratio.

In most radar applications, the clutter power received by a system is unwanted and often treated as noise. In this application, the clutter power (P_c) was treated as the return from a desired target. The clutter power for a bistatic system given by Skolnik (15:557).

$$P_c = \frac{P_t G_t G_r \lambda^2 \sigma_b}{(4\pi)^3 D_t^2 D_r^2 L_p(t) L_p(r) L_s} \quad (2.1)$$

Where:

P_r =clutter power received

G_t =transmitting antenna gain in the direction of the clutter

G_r =receiving antenna gain in the direction of the clutter

σ_b =bistatic radar cross section of the clutter

D_t =transmitter to target distance

D_r =receiver to target distance

$L_p(t)$ =propagation loss over the transmitter to target path

$L_p(r)$ =propagation loss over the receiver to target path

L_s =system losses

A majority of the parameters in Equation 2.1 are known or can be calculated given enough information about the transmitting hardware, receiving hardware, and physical layout of the bistatic system. The only factor intimately associated with the terrain characteristics is σ_b which represents the bistatic RCS of the target. For many simple geometric shapes the RCS is known or can be calculated with reasonable accuracy. The problem at hand is that the target of interest is terrain of varying degrees of roughness populated by objects of random shapes, sizes, heights and densities.

The randomness of the problem requires a probabilistic approach to determining a value for σ_b in realistic terrains encountered by a bistatic radar system. The value obtained for σ_b is directly related to the physical dimensions of the clutter patch illuminated by the transmitted signal and simultaneously visible to the receiving antenna's aperture. Once the visible footprint is identified, other factors can influence the amount of clutter power received from the footprint.

2.2.1 Factors Affecting the Clutter Power. The other factors which affect the amount of clutter power received include the type of land cover found in the footprint area, the density of the land cover, the variation in the surface heights and slopes of the land as well as the variation in the heights and slopes of the objects populating the surface.

In addition to the physical locations of objects in the target area, one must also consider the electrical properties of these objects. The dielectric constants of both the terrain surface in a clutter cell and of the objects populating the cell affect the average amount of scattered power reaching the receiver aperture.

The average clutter power received will also depend upon the incident angle of the illuminating wave (θ_i), the angle of departure of the scattered wave (θ_s), and the bistatic angle (β) formed by the transmitter, receiver, and target area. The angles θ_i , θ_s , and ϕ_s are defined at the point of incidence as shown in Figure 2.1 and the

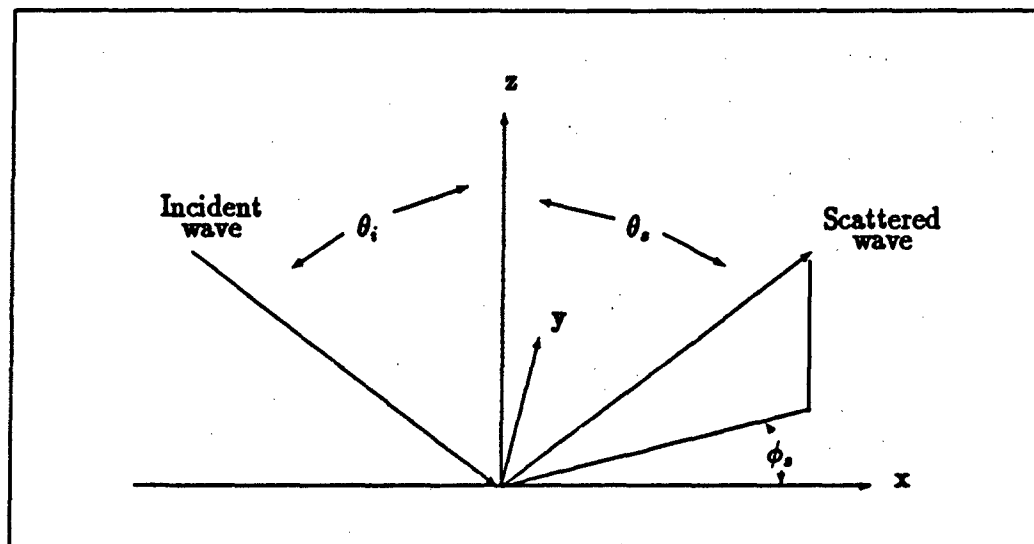


Figure 2.1. Bistatic scattering geometry.

bistatic angle, β , is defined as $\pi - \phi_s$.

Still other factors can affect the amount of scattered energy received from the clutter cell. The homogeneity of the surface composition in the clutter cell can affect the signal contribution from the slightly rough and very rough surface contributions. The size of the clutter cell blocks can have the same effect on the signal levels as the homogeneity of the surface. Surfaces which have small homogeneous sections of many different types of surface present a problem when trying to determine the dominant material in a clutter cell block. The same situation is possible if the size of the clutter cell blocks are too large.

Weather conditions can change the reflectivity of an area in a matter of minutes. Windy conditions can cause the RMS height of crops to vary drastically or cause portions of trees to move in and out of a particular range cell block. Rain can affect most surface areas by changing the surface moisture content. Snow and ice cover can totally change the reflection characteristics of a surface area.

Some factors cause seasonal change. Areas covered by vegetation will have an RMS height which will change as the vegetation grows over the summer or is har-

vested in the fall. Similarly, forested areas of deciduous trees will have a reflectivity which will change seasonally as leaves appear in spring, grow throughout the summer and drop off in autumn.

The previous discussion was intended to point out that there is no single solution to the problem of predicting the bistatic reflectivity of a given area. So many factors can affect the results that it is only feasible to estimate the value of clutter power for a given set of conditions. The estimate must be revised as the conditions change. The first obstacle to overcome in providing this estimate is identifying the clutter cell location.

2.3 Determining the Antenna Footprint.

The terrain area which scatters electromagnetic energy that reaches the receiver during any particular range gate period is of primary interest. Determination of these terrain sections is the foundation for all subsequent scattering calculations. Each clutter cell is delimited by two features, the bistatic equirange contour lines for a specific receiver range gate period and the intersection of the transmitter and receiver antenna patterns. The equirange contour lines establish the areas of possible energy return during a range gate period. The transmitter and receiver antenna patterns are then used to identify subsections of the range cell which make significant contributions to the received clutter power.

2.3.1 The Equirange Contour Lines. Figure 2.2 represents a two dimensional view of the bistatic geometry from which it is desired to determine the dimensions of the individual range cells. In this diagram the transmitter, receiver, and target are in the same plane and variations in surface height are being neglected for the moment. This is the same situation one is faced with when extracting data from a topographic map.

The angle β is the bistatic angle. The segment D_B is the baseline distance in the

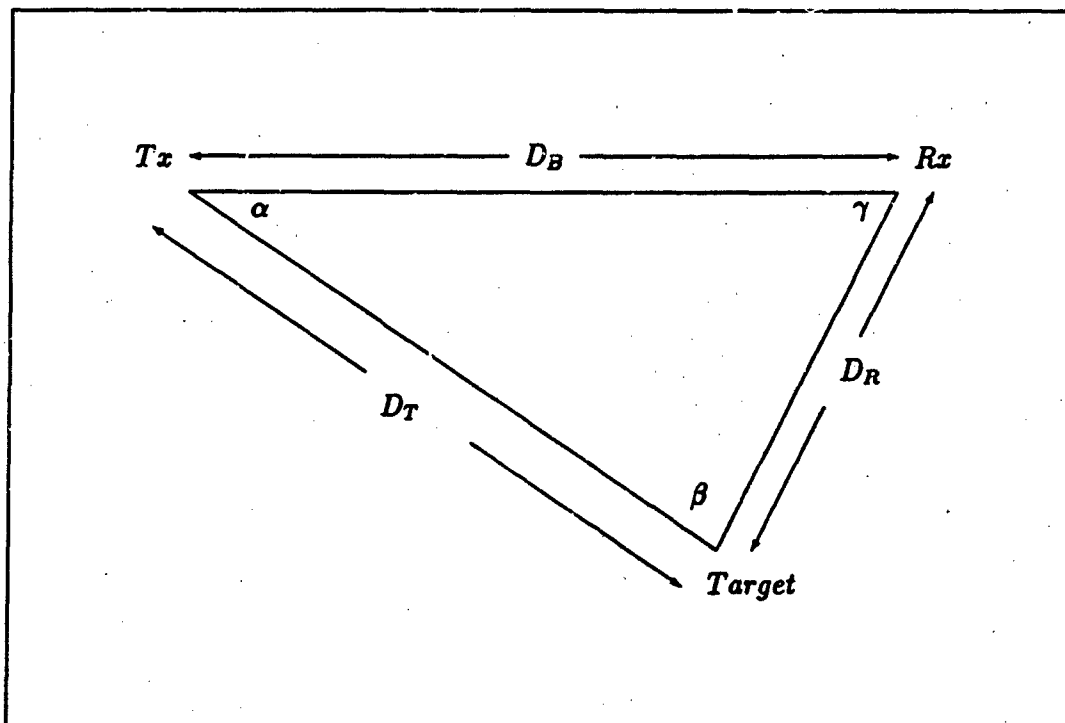


Figure 2.2. Two dimensional bistatic geometry.

xy-plane from transmitter to receiver and remains constant for a given ground based bistatic system. The segment D_T is the distance in the xy-plane from transmitter to a selected range cell. The segment D_R is the distance in the xy-plane from the selected range cell to the receiver. Both segments, D_R and D_T , will vary in length with different range cells.

The amount of clutter power detected by the receiver from each range cell will be equal to the average of the energy intercepted by the receiver during a single range gate period. Therefore the width of the range cell is related to the range gate interval of the receiver. The number of range cells available is controlled by the transmitter PRF. The easiest way to visualize this is to examine a timing diagram for the system.

Figure 2.3.1 is a timing diagram for the general ground based bistatic system.

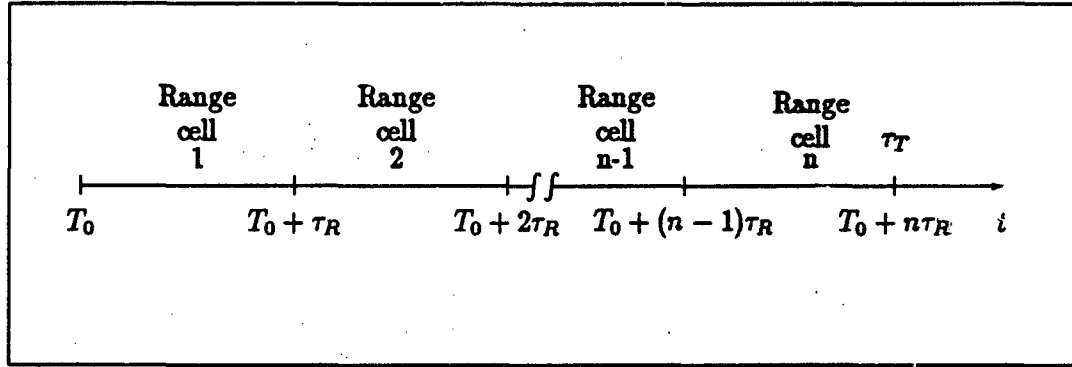


Figure 2.3. Ground based bistatic system timing diagram.

The timing diagram is referenced to the receiver. At time T_0 , energy traveling along a direct path, the distance R_B , reaches the receiver. Where R_B is the line of sight (LOS) or slant range distance from the transmitter to the receiver. In Figure 2.3.1 τ_R represents the range gate interval of the receiver. The energy for range cell one strikes the receiver between time T_0 and $T_0 + \tau_R$. Similarly the energy for range cell two strikes the receiver antenna between $T_0 + \tau_R$ and $T_0 + 2\tau_R$. The total number of range cells, n , is determined by the PRF of the transmitter. In Equation 2.2 $\tau_T = \frac{1}{PRF}$ has been used.

$$n = \frac{1}{(PRF)(\tau_R)} = \frac{\tau_T}{\tau_R} \quad (2.2)$$

The shape of a clutter cell for a bistatic system is more complicated than its monostatic counterpart. The most direct method for determining the shape of a clutter cell is to examine the equirange contour lines for a bistatic system. For any arbitrary n^{th} equirange contour line, energy reaches the receiver after a time of $T_0 + n\tau_R$ seconds. The distance traveled by this energy is equal to the sum of the transmitter to target and target to receiver distances. An equivalent LOS distance can be determined from the wave speed and time of travel. At the time of the n^{th} range gate, the wave has been traveling for a period of $T_0 + n\tau_R$ seconds. Equating

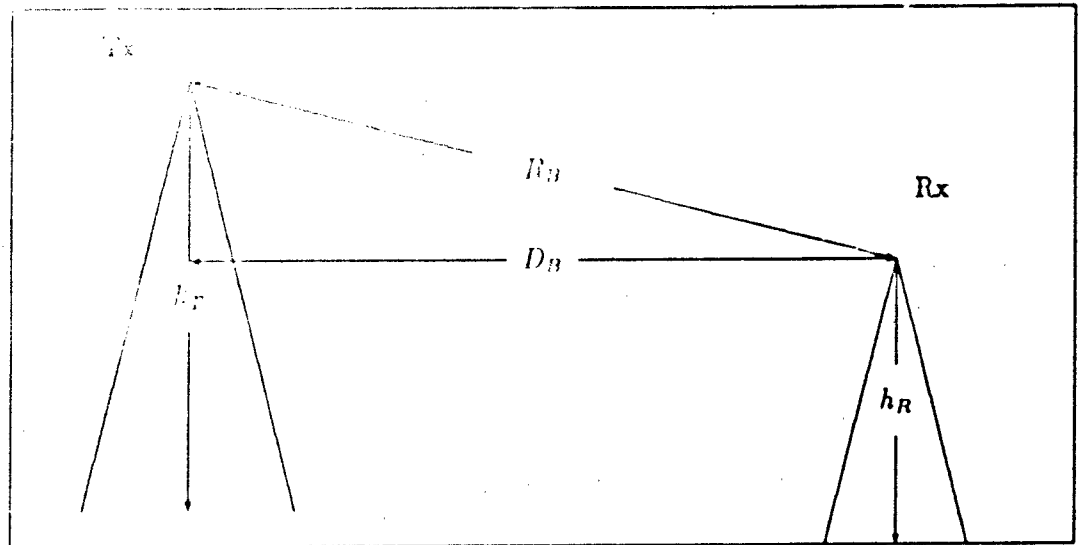


Figure 2.4. Relationship between slant ranges and xy-plane distances.

these facts yields:

$$R_T + R_R = c(T_0 + n\tau_R) = R_B + nc\tau_R \quad (2.3)$$

The right hand side of Equation 2.3 is a constant value for any given value of n and τ_R , the receiver range gate interval. If the transmitter is assumed to be an isotropic radiator, energy is radiated in all directions. By plotting the target points for all directions radially from the transmitter and determining the values for R_T and R_R which satisfy Equation 2.3, these equirange contour lines will be elliptical in shape. However R_T and R_R are the slant ranges from the transmitter to target and receiver to target respectively and can not be directly plotted on a topographic map.

Figure 2.4 illustrates the relationship between the LOS slant ranges (R_B , R_T , R_R) and their corresponding xy-plane distances (D_B , D_T , D_R) related to the topographic map.

In Figure 2.4, the transmitter and receiver are located atop surface heights h_T and h_R respectively, which are measured from a sea level xy-plane. By letting the difference in height be $\delta h_B = |h_T - h_R|$, R_B can be expressed as:

$$R_B = \sqrt{(\delta h_B)^2 + (D_B)^2} \quad (2.4)$$

Similarly D_B can be expressed in terms of R_B and δh_B as:

$$D_B = \sqrt{(R_B)^2 - (\delta h_B)^2} \quad (2.5)$$

By defining $\delta h_T = |h_T - h_c|$ and $\delta h_R = |h_R - h_c|$ where h_c is the height of the clutter at the point of reflection, expressions similar to Equations 2.4 and 2.5 can be derived for R_T, R_R, D_T , and D_R .

$$R_T = \sqrt{(\delta h_T)^2 + (D_T)^2} \quad (2.6)$$

$$D_T = \sqrt{(R_T)^2 - (\delta h_T)^2} \quad (2.7)$$

$$R_R = \sqrt{(\delta h_R)^2 + (D_R)^2} \quad (2.8)$$

$$D_R = \sqrt{(R_R)^2 - (\delta h_R)^2} \quad (2.9)$$

A plot of the equirange contour lines is illustrated in Figure 2.5. The concentric ellipses have the transmitter and receiver as focal points. For any range gate interval, it is possible for the target clutter cell to include any of the area between the corresponding equirange ellipses. The goal of this research is to determine the bistatic clutter power from the topography of the area surrounding the system. Therefore,

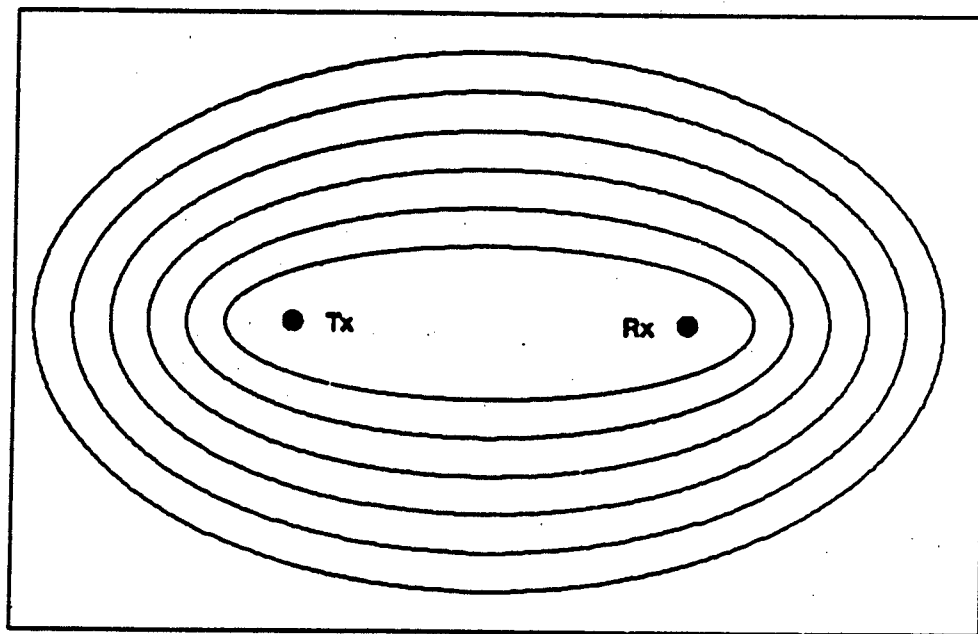


Figure 2.5. equirange contour lines for a ground based bistatic system.

a process is needed to identify any or all of the equirange contours for a given radar system on a topographic map of the area surrounding the system.

Figure 2.6 was partially extracted from Beyer (4:198) and illustrates the basic geometry for any ellipse. For an ellipse centered at point (h,k) with its major axis parallel to the x axis of a cartesian coordinate system, Beyer (4:199) lists the following expression for the ellipse:

$$\frac{(x-h)^2}{a^2} + \frac{(y-k)^2}{b^2} = 1 \quad (2.10)$$

Expressing a , b , h , and k from Equation 2.10 in terms of the known system parameters τ_R , D_B , D_T , D_R , and n will allow the delineation of the equirange contour lines on the topographic map. For convenience we choose a coordinate system centered on the transmitter with the x axis collinear with the slant range R_B .

For any ellipse, the sum of the distances from any point on the ellipse to the foci equals the distance $2a$ in Figure 2.6 (4:199). Applying this principle to Figure 2.7

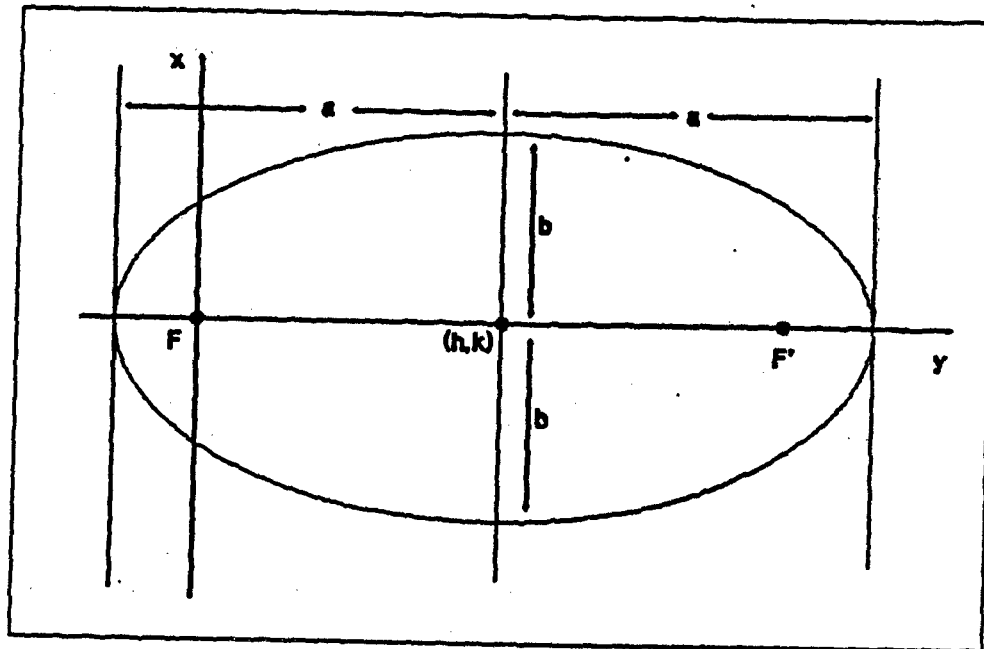


Figure 2.6. Basic geometry for an ellipse.

where the distances from any point on the equirange contour to the foci are R_T and R_R yields:

$$a = \frac{R_T + R_R}{2} \quad (2.11)$$

From Equation 2.3 it was shown that $R_T + R_R$ is equal to $R_B + ncr_B$. Substituting this into Equation 2.11 yields:

$$a = \frac{R_B + ncr_B}{2} \quad (2.12)$$

Beyer (4:199) states that the distance from the center of the ellipse to either foci, d_{cf} , is given by:

$$d_{cf} = \sqrt{a^2 - b^2} \quad (2.13)$$

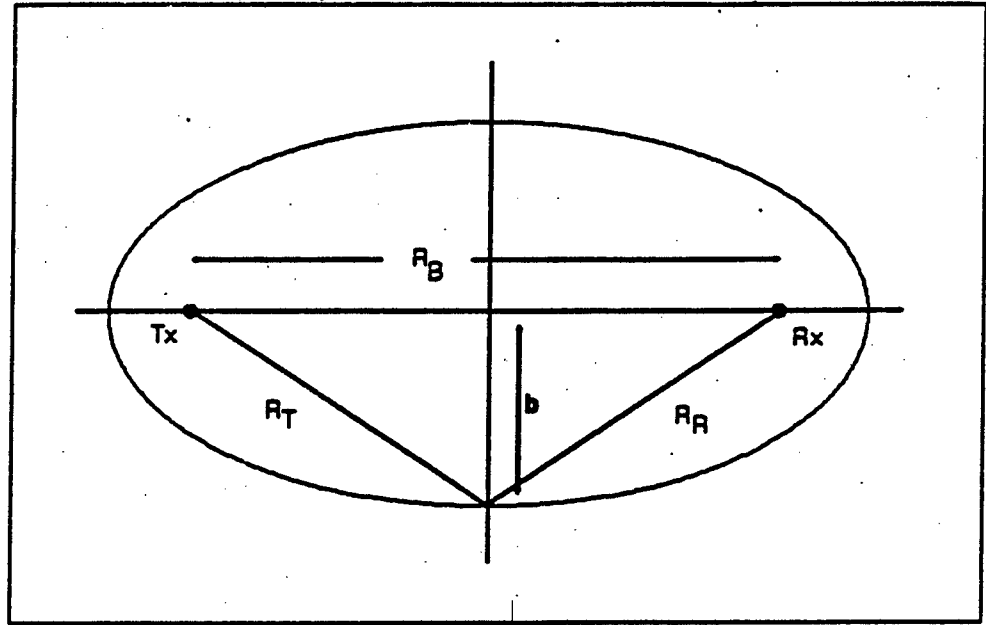


Figure 2.7. Geometry for the case when $R_T = R_R$.

From Figure 2.6 it is clear that the distance d_{cf} is equal to $R_B/2$. Substituting $R_B/2$ into Equation 2.13 for d_{cf} and the right hand side of Equation 2.12 for a , simplifying and solving for b yields:

$$b = \frac{\sqrt{n\epsilon_T R (2R_B + n\epsilon_T R)}}{2} \quad (2.14)$$

Substituting these expressions for a and b given by Equations 2.12 and 2.14 into Equation 2.10 and noting that $k = 0$ for the geometry shown in Figure 2.6 yields:

$$\frac{4(x-h)^2}{(R_B + n\epsilon_T R)^2} + \frac{4y^2}{n\epsilon_T R (2R_B + n\epsilon_T R)} = 1 \quad (2.15)$$

Rearranging terms in Equation 2.15 and solving for y yields:

$$y = \frac{\sqrt{n\epsilon_T R (2R_B + n\epsilon_T R) [(R_B + n\epsilon_T R)^2 - 4(x-h)^2]}}{2(R_B + n\epsilon_T R)} \quad (2.16)$$

Using Equation 2.16 the magnitude and direction of R_T can be determined by:

$$R_T = \sqrt{y^2 + x^2} \quad (2.17)$$

$$\theta_{R_T} = \arctan \frac{y}{x} \quad (2.18)$$

Substituting Equation 2.17 and $\delta h_T = |h_T - h_c|$ into Equation 2.7 yields an equation which can be used to determine an exact value for D_T which in turns identifies two points on an equirange contour line on the topographic map.

$$D_T = \sqrt{x^2 + y^2 - (h_T - h_c)^2} \quad (2.19)$$

Using Equation 2.19 to identify equirange contour lines on a topographic map can become a very time consuming process because use of the equation is iterative in nature. For a selected value of x , a corresponding y is calculated. These values along with the known transmitter site height, h_T , can then be used with Equation 2.19 to determine D_T from the clutter heights, h_c , along the direction given by Equation 2.18. The process is a trial and error procedure when completed manually in search of the values of D_T and h_c which satisfy the equation. If digitized surface height data were available the process could be automated, but this is not the case.

An alternative is to establish an acceptable level of error in D_T and identify the conditions where D_T can be approximated by R_T . R_T is easily identified and can be plotted directly on the topographic map by using Equations 2.16.

Let the error associated with assuming that D_T can be approximated by R_T be denoted by e_{RD} where e_{RD} is defined as:

$$e_{RD} = \frac{R_T - D_T}{R_T} \quad (2.20)$$

The maximum width of any clutter cell will occur along the major axis of the equirange ellipses which define the cell. For an arbitrary n^{th} clutter cell, the distance traveled by the wave from the transmitter to the leading edge of the ellipse defining the cell is $c(T_0 + (n-1)\tau_R/2)$. Similarly, the distance traveled by the wave to the outermost ellipse which defines the n^{th} clutter cell is $c(T_0 + n\tau_R/2)$. Therefore the maximum width of the n^{th} clutter cell is given by:

$$W_c = c\left(T_0 + \frac{n\tau_R}{2}\right) - c\left(T_0 + \frac{(n-1)\tau_R}{2}\right) = \frac{c\tau_R}{2} \quad (2.21)$$

The criterion for determining the quality of the $D_T \approx R_T$ assumption will be how much error is introduced into the width of the clutter cell and in turn the location of the clutter cell delimiting ellipses. Letting the P represent a numerical percentage expression the condition for the assumption is stated as:

$$e_{rd} \leq PW_c \quad (2.22)$$

Substituting Equations 2.21, 2.20, and 2.7 into Equation 2.22 yields:

$$\frac{R_T - \sqrt{(R_T)^2 - (\delta h_T)^2}}{R_T} \leq \frac{Pc\tau_R}{2} \quad (2.23)$$

Substituting $\delta h_T = \sqrt{(h_T - h_c)^2}$ into Equation 2.23 and solving for h_c yields:

$$h_c \leq c\tau_R \sqrt{P[2R - P(c\tau_R)^2]} + h_T \quad (2.24)$$

By specifying a percentage of the total range cell width, P , as an allowable error, Equation 2.24 can be used to identify a range of clutter heights, h_c , which allow D_T to be approximated by R_T . For areas which meet the conditions established by Equation 2.24, Equations 2.16 and 2.17 can be used to identify the perimeters of specific range cells.

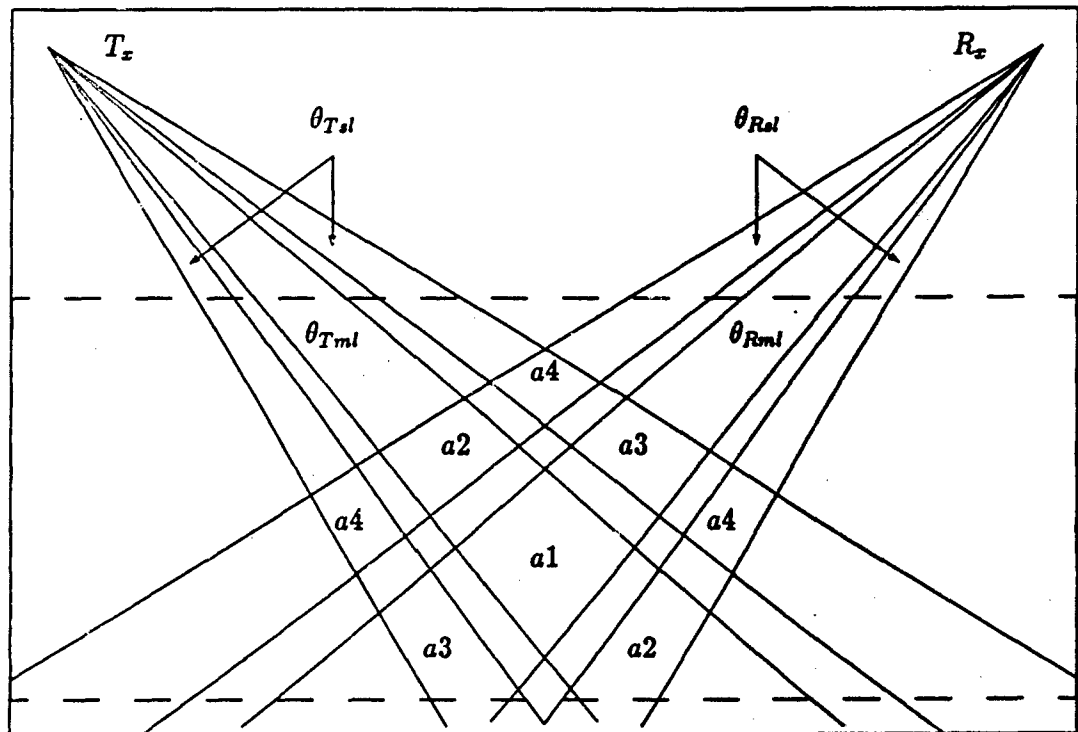


Figure 2.8. Clutter Blocks Created by the Antenna Patterns.

2.3.2 The Antenna Patterns. Once the equirange contour lines have been identified, the actual shape of the target area which contributes to the clutter power detected at the receiver can be determined by overlaying the the system antenna patterns as illustrated in Figure 2.8. In this research project, the main beam patterns as well as the significant side lobe patterns will be considered. In Figure 2.8 θ_{Tml} and θ_{Rml} represent the 3 dB beamwidths of the transmitting and receiving antennas main lobes. The notation used is similar for the side lobes. The side lobe beamwidths represented by θ_{Tsl} and θ_{Rsl} are determined by the width of the side lobes at points where their power has decreased to 3 dB below maximum. The dashed lines represents the equirange contour lines which delimit the range cell.

The impact of including the side lobe patterns is that a particular range cell may include up to nine individual clutter blocks which act as sources of scattered

energy as opposed to a single clutter block when only the main beams are considered. The additional clutter blocks are a result of the interaction of the main and side lobes of the two antennas. Each antenna pattern intersection in a single range cell will be treated as a separate clutter cell as shown in Figure 2.8. Here the individual clutter cells are labeled a_1, a_2, a_3 , and a_4 to identify the different possible combinations of gains and beamwidths.

In the diagram, a_1 represents the intersection of both main beam patterns while a_2 identifies the intersection of the transmitters main lobe and the receivers side lobes. Similarly, a_3 identifies the receiver main lobe to transmitter side lobe intersection and a_4 the side lobe to side lobe intersections.

The number of additional clutter blocks to be considered will depend on the width of the range cell, the bistatic angle, the base line distance between the transmitter and receiver and the individual antenna patterns. Note that in Figure 2.8 the range cell shown has only eight clutter blocks. This situation will not arise for the system used in this research because of the narrow transmitter beam width and the short distances between the transmitter, receiver, and target area.

Each clutter cell may have to be further subdivided into blocks and analyzed individually. The analysis of the target area terrain involves identifying the heights those areas which exhibit similar roughness characteristics and surface cover. Each similar block of surface area was analyzed to determine the mean and variance of the heights and a height distribution which best describes the block. From these characteristics it was possible to calculate the RCS for each target area block. For those clutter cells which engulf more than one type of surface area, the cell will be further subdivided into clutter blocks corresponding to the respective target area blocks. The RCS from each target area block can then be used with the area of the clutter block to determine the power contribution from that clutter block. The total power from the clutter cell will be the sum of the powers from the individual clutter blocks.

The notation used in Figure 2.8 is not meant to imply that all clutter cells labeled similarly will have the same type of height distribution or even identical physical areas. This requires that the receiver clutter power formula given by Equation 2.1 be modified to replace a single transmitter gain, receiver gain, and bistatic cross section with summations as shown below to account for the multiple gain and cross section products.

$$P_c = \frac{P_t \lambda^2 \left(G_{Tm} G_{Rm} \sigma_{ba1} + G_{Tm} G_{Rs} \sum_{i=1}^2 \sigma_{ba2i} + G_{Ts} G_{Rm} \sum_{j=1}^2 \sigma_{ba3j} + G_{Ts} G_{Rs} \sum_{k=1}^4 \sigma_{ba4k} \right)}{(4\pi)^3 D_t^2 D_r^2 L} \quad (2.25)$$

Where:

G_{Tm} = gain in transmitter main lobe

G_{Ts} = gain in transmitter side lobe

G_{Rm} = gain in receiver main lobe

G_{Rs} = gain in receiver side lobe

σ_{ba1} = cross section of $a1^{th}$ clutter cell

2.4 Determining the Incoherent Contribution Power.

2.4.1 Rough Surface Models. Many models exist which describe scattering from rough surfaces (3:70-99), (13:671-753), (9:75-89). The most general of these is presented by Barrick (13:703-729). He addresses two specific cases for incoherent scattering, slightly rough surfaces and very rough surfaces. The approach varies for determining the normalized RCS depending upon the roughness of the surface. Barrick denotes the scattering coefficient as $\gamma(\theta_i, \theta_s, \phi_s)$ (13:672) which he defines as:

$$\gamma(\theta_i, \theta_s, \phi_s) = \frac{\langle \sigma(\theta_i, \theta_s, \phi_s) \rangle}{A} \quad (2.26)$$

Where:

A = The area of the terrain surface being characterized.

$\langle \sigma(\theta_i, \theta_s, \phi_s) \rangle$ = The average RCS of the surface in question.

It is apparent from Equation 2.26 that Barrick's $\gamma(\theta_i, \theta_s, \phi_s)$ is often denoted as σ^0 the normalized Radar cross section (NRCS) by other authors. For a given target area, Equation 2.26 will have to be used for each section of the target area that displays different height or surface cover characteristics. The target area composed of homogeneous characteristics used to determine the RCS of the area may not be totally illuminated by the wave front for a single range cell. The RCS in Equation 2.1 is the total cross section of a single range cell. Therefore σ_0 for a given range cell is given by:

$$\sigma_0 = \gamma(\theta_i, \theta_s, \phi_s) A_c = \langle \sigma(\theta_i, \theta_s, \phi_s) \rangle \quad (2.27)$$

Where:

A_c is the area of the terrain illuminated by the wavefront which corresponds to a given range cell.

Two assumptions stated by Barrick (13:672) are: $D_i D_r \gg A$, the product of the target to transmitter/receiver distances must be greater than the area of the terrain characterization surface in question, and $\lambda^2 \ll A$, the operating wavelength must be much less than the area of the terrain characterization surface. These assumptions can be used to set limits on the size of the homogeneous areas of terrain used to develop the terrain statistics ($\lambda^2 \ll A \ll D_i D_r$).

The roughness scale is determined by comparing the rms height of the surface (h) to the wavelength (λ) of the signal being transmitted. For cases where $h \ll \lambda$, the surface is considered to be slightly rough. When $h \gg \lambda$, the surface is considered as a very rough surface.

2.4.2 *Incoherent Scattering From a Slightly Rough Surface.* Barrick (13:703-706) explains incoherent scattering from a slightly rough homogeneous surface as:

$$\gamma_{pq} = \frac{4}{\pi} k_0^4 h^2 \cos^2 \theta_i \cos^2 \theta_s |\alpha_{pq}|^2 I \quad (2.28)$$

Where p and q represent the polarization state of the incident and scattered waves. In Equation 2.28 the quantity I was defined as follows:

$$I = \int_0^\infty r \rho(r) J_0(r k_0 \sqrt{\xi_x^2 + \xi_y^2}) dr = \frac{\pi^2}{h^2} u(k_0 \sqrt{\xi_x^2 + \xi_y^2}) \quad (2.29)$$

In Equation 2.29 ξ_x , ξ_y , $\rho(r)$, and r are defined as:

$$\xi_x = \sin \theta_i - \sin \theta_s \cos \phi_s \quad (2.30)$$

$$\xi_y = \sin \theta_s \sin \phi_s \quad (2.31)$$

$$\rho(r) = \frac{\langle \zeta(x, y) \zeta(x', y') \rangle}{h^2} \quad (2.32)$$

$$r = \sqrt{(x - x')^2 + (y - y')^2} \quad (2.33)$$

Equation 2.32 is the surface height correlation coefficient. In order to use Equation 2.29 the distribution of the surface heights must be known or a height distribution must be assumed. The two most commonly used distributions (13:704) are Gaussian and two sided exponential. A Gaussian surface height distribution will be assumed for the work accomplished during this research. Based on this assumption, Equation 2.32 becomes:

$$\rho(r) = \exp \left(\frac{-r^2}{l^2} \right) \quad (2.34)$$

Substituting Equation 2.34 into Equation 2.29 and carrying out the integration yields:

$$I = \pi l^2 \exp \left[\frac{-k_0^2 l^2 (\xi_x^2 + \xi_y^2)}{4} \right] \quad (2.35)$$

Where the quantity l in Equations 2.34 and 2.35 represents the correlation distance, the distance required to cause the correlation function to reach a value of $1/e$.

The final term required for Equation 2.28 is an expression for the α_{pq} term. As previously stated, only linear polarizations are to be considered here, therefore the only terms which apply to the task at hand are α_{hh} and α_{vv} . The terms are defined by Barrick (13:706) as:

$$\alpha_{hh} = \frac{(\mu_r - 1) \left(\mu_r \sin \theta_i \sin \theta_s - \cos \phi_s \sqrt{\epsilon_r \mu_r - \sin^2 \theta_i} \sqrt{\epsilon_r \mu_r - \sin^2 \theta_s} \right) + \mu_r^2 (\epsilon_r - 1) \cos \phi_s}{\left(\mu_r \cos \theta_i + \sqrt{\epsilon_r \mu_r - \sin^2 \theta_i} \right) \left(\mu_r \cos \theta_s + \sqrt{\epsilon_r \mu_r - \sin^2 \theta_s} \right)} \quad (2.36)$$

$$\alpha_{vv} = \frac{(\epsilon_r - 1) \left(\epsilon_r \sin \theta_i \sin \theta_s - \cos \phi_s \sqrt{\epsilon_r \mu_r - \sin^2 \theta_i} \sqrt{\epsilon_r \mu_r - \sin^2 \theta_s} \right) + \epsilon_r^2 (\mu_r - 1) \cos \phi_s}{\left(\epsilon_r \cos \theta_i + \sqrt{\epsilon_r \mu_r - \sin^2 \theta_i} \right) \left(\epsilon_r \cos \theta_s + \sqrt{\epsilon_r \mu_r - \sin^2 \theta_s} \right)} \quad (2.37)$$

Where:

ϵ_r = The relative permittivity of the target area.

μ_r = The relative permeability of the target area.

Equations 2.36 and 2.37 can be simplified by assuming that objects in the target area will probably consist of nonmagnetic materials. This implies that $\mu_r \approx 1$ and Equations 2.36 and 2.37 can be recast as:

$$\alpha_{hh} = -\frac{(\epsilon_r - 1) \cos \phi_s}{\left(\cos \theta_i + \sqrt{\epsilon_r - \sin^2 \theta_i}\right) \left(\cos \theta_s + \sqrt{\epsilon_r - \sin^2 \theta_s}\right)} \quad (2.38)$$

$$\alpha_{vv} = \frac{(\epsilon_r - 1) \left(\epsilon_r \sin \theta_i \sin \theta_s - \cos \phi_s \sqrt{\epsilon_r - \sin^2 \theta_i} \sqrt{\epsilon_r - \sin^2 \theta_s} \right)}{\left(\epsilon_r \cos \theta_i + \sqrt{\epsilon_r - \sin^2 \theta_i} \right) \left(\epsilon_r \cos \theta_s + \sqrt{\epsilon_r - \sin^2 \theta_s} \right)} \quad (2.39)$$

The incoherent scattering from slightly rough surfaces typically is caused by the material covering the terrain surface like grass, crops, and foliage. A detailed description of these items is required to develop a statistical characterization of their heights and composition. Unfortunately, this type of information is not available from topographic maps.

The maps do provide a general description of the type of land cover in categories like forest, swamp, sand etc. More specific information about the ground cover is required to implement the procedure outlined in this section therefore, incoherent scattering from slightly rough surfaces will not be demonstrated in this report.

2.4.3 Incoherent Scattering From Very Rough Surfaces As the roughness of the surface increases, the scattered power attains more contribution from the incoherently scattered power and less from the coherently scattered power. Barrick states (13:719) for $k_0 h > 5$ the scattered power is essentially incoherent.

The approach for deriving the very rough surface solutions differs from the slightly rough surface approach. The principle of physical optics was used by Barrick to solve the Stratton-Chu integral equation to describe the scattering from very rough surfaces. His derivation and analysis are based on the tangent plane approxi-

mation to identify the surface current present on a finite section of terrain to solve the integral equation. A statistical representation of the randomly oriented terrain surface heights is required to express the scattering as specular reflection from the random surfaces in the target area (13:719). His approach (13:720) invokes the following restrictions:

1. The radius of curvature $\gg \lambda$.
2. The roughness is isotropic.
3. The correlation length $l \ll \sqrt{\lambda}$.
4. The effects of multiple scattering and shadowing were neglected.

Based upon these assumptions, the average NRCS as derived by Barrick (13:720) is given by:

$$\gamma_{rq} = |\beta_{rq}|^2 J \quad (2.40)$$

In Equation 2.40 β_{rq} and J are analogous to the quantities α_{rq} and I for the slightly rough surface. Where J is defined by Barrick as:

$$J = 2k_0^2 \int_0^\infty r J_0(r k_0 \sqrt{\xi_x^2 + \xi_y^2}) M_{\zeta\zeta'}(iK_0\xi_x, -iK_0\xi_x; r) dr \quad (2.41)$$

Where:

$J_0(x)$ is a zero order cylindrical Bessel function.

ζ and ζ' are surface height random variables separated a distance r .

$M_{\zeta\zeta'}(iu, iv; r)$ is the joint characteristic function of the surface height random variables.

This joint characteristic function is the Fourier transform of the joint probability density function (JPDF), $P_J(\zeta, \zeta')$, which describes the surface heights. As

with the I function from Equation 2.29 for the slightly rough surface, the density function describing the heights must be known or assumed to calculate a value for the J function. This JPDF will again be assumed to be Gaussian and given by:

$$P_J(\zeta, \zeta') = \frac{1}{2\pi h^2 [1 - \rho^2(r)]^{\frac{1}{2}}} \exp \left\{ -\frac{[\zeta^2 - 2\zeta\zeta'\rho(r) + (\zeta')^2]}{2h^2 [1 - \rho^2(r)]} \right\} \quad (2.42)$$

In Equation 2.42, ζ and ζ' represent the surface heights at two locations (x, y) and (x', y') and $\rho(r)$ represents the Gaussian correlation function given by:

$$\rho(r) = \exp \left(\frac{-r^2}{l^2} \right) \quad (2.43)$$

Where:

$r^2 = (x - x')^2 + (y - y')^2$ The distance between two points.

l^2 = The square of the correlation distance.

Barrick (13:721) argues that the Gaussian correlation coefficient, Equation 2.43, can be expressed by the first two terms of a power series expansion for his development of the high frequency scattering model as:

$$\rho_r \approx 1 - \frac{r^2}{l^2} \quad (2.44)$$

Using the Gaussian surface height JPDF given in Equation 2.42 and the small signal approximation for the Gaussian surface height correlation function given in Equation 2.43 in Equation 2.41 yields the following expression after integration:

$$J = \frac{4}{s^2 \xi_z^2} \exp \left[-\frac{1}{s^2} \left(\frac{\xi_x^2 + \xi_y^2}{\xi_z^2} \right) \right] \quad (2.45)$$

Where the quantities in Equation 2.45 s^2 , ξ_x , ξ_y , and ξ_z have been defined as:

$$\xi_x = \sin \theta_i - \sin \theta_r \cos \phi_s \quad (2.46)$$

$$\xi_y = \sin \theta_i \sin \phi_s \quad (2.47)$$

$$\xi_z = -\cos \theta_i - \cos \phi_s \quad (2.48)$$

$$s^2 = \frac{4h^2}{l^2} \quad (2.49)$$

Where:

h^2 is the mean squared roughness height.

l is the surface correlation length.

The scattering matrix in Equation 2.40 is represented by β_{pq} , where again the subscripts p and q denote the polarization state of the transmit and receive antennas respectively. In this research, only vertical and horizontal linear polarizations were considered and the scattering matrix elements were defined as:

$$\beta_{vv} = \frac{a_2 a_3 R_{||}(z) + \sin \theta_i \sin \theta_r \sin^2 \phi_s R_{\perp}(z)}{a_1 a_4} \quad (2.50)$$

$$\beta_{hh} = \frac{-\sin \theta_i \sin \theta_r \sin^2 \phi_s R_{||}(z) - a_2 a_3 R_{\perp}(z)}{a_1 a_4} \quad (2.51)$$

The expressions $R_{\perp}(z)$ and $R_{||}(z)$ are modified Fresnel reflection coefficients given by the following expressions:

$$R_{||}(z) = \frac{\epsilon_r \cos z - \sqrt{\epsilon_r \mu_r - \sin^2 z}}{\epsilon_r \cos z + \sqrt{\epsilon_r \mu_r - \sin^2 z}} \quad (2.52)$$

$$R_{\perp}(i) = \frac{\mu_r \cos i - \sqrt{\epsilon_r \mu_r - \sin^2 i}}{\mu_r \cos i + \sqrt{\epsilon_r \mu_r - \sin^2 i}} \quad (2.53)$$

The angle i used in Equations 2.52 and 2.53 has been defined as follows by Barrick:

$$\cos i = \frac{1}{\sqrt{2}} \sqrt{1 - \sin \theta_i \sin \theta_s \cos \phi_s + \cos \theta_i \cos \theta_s} \quad (2.54)$$

The quantities a_1 , a_2 , a_3 , and a_4 used in Equations 2.50 and 2.51 have been defined as follows:

$$a_1 = 1 + \sin \theta_i \sin \theta_s \cos \phi_s - \cos \theta_i \cos \theta_s \quad (2.55)$$

$$a_2 = \cos \theta_i \sin \theta_s + \sin \theta_i \cos \theta_s \cos \phi_s \quad (2.56)$$

$$a_3 = \sin \theta_i \sin \theta_s + \cos \theta_i \sin \theta_s \cos \phi_s \quad (2.57)$$

$$a_4 = \cos \theta_i + \cos \theta_s \quad (2.58)$$

By using the expressions given above, the NRCS of a selected block of terrain which meets all the restrictions listed can be calculated for any given bistatic geometry. The NRCS can then be multiplied by the area of this terrain which is illuminated by both transmitting and receiving antennas for a particular range cell to determine the the RCS. Once the RCS is known, the scattered power from the section of terrain can be determined by using Equation 2.25.

III. Application of the Process and Results

3.1 Known System Parameters.

In this chapter the process described in Chapter II will be applied to a ground based bistatic system operated by the sponsor, RADC/EECE. The process elements which can be implemented from information obtained from topographic maps will be illustrated and results presented. The starting point is to identify all known parameters for the system in question.

The transmitting hardware is a pulsed 3 GHz S band weather radar system located near Stow Massachusetts and operated by the Air Force Geophysics Laboratory (AFGL). The transmitter radiates a peak power of 800 KW using a 28 foot parabolic dish antenna. The antenna is located atop a 15 foot tower on a hill top which has an elevation of approximately 93 meters, therefore the quantity $h_T \approx 97.572$ meters. The transmitter has a PRF of 1 KHz and a pulse width of $1 \mu S$. The beam width of the antenna's main lobe was estimated by the sponsor to be approximately 1° .

The receiving hardware is located atop Prospect Hill in Waltham Massachusetts and employs a standard gain 20 dB horn antenna. Prospect Hill is approximately 144 meters above sea level, therefore the quantity $h_R \approx 144$ meters. The receiver is capable of operating with a variety of range gate intervals but will use a $1 \mu S$ interval for this project, therefore the quantity $\tau_R = 1 \mu S$.

The linear distance between the transmitter and receiver sites is 19.248 Km and the baseline slant range can be determined from Equation 2.4 using $h_T = 97.572$, $h_R = 144$, and $D_B = 19248$. Performing the calculation yields $R_B \approx D_B = 19248$ meters.

3.2 Establishing the Clutter Cells.

To establish the clutter cells three patterns must be identified. The equirange contour lines must be identified on the topographic map. In addition both antenna patterns must be identified. The intersection of the antenna patterns and a particular range cell identifies the clutter cell dimension applicable to that particular range cell.

3.2.1 Identifying the Equirange Contour Lines. The first step is to determine the equirange contour lines. Both sites are located on a single USGS topographic map, The Maynard Massachusetts 7.5 by 15 minute map. A rectangular coordinate system was established on the topographic map such that the transmitter site was located at the origin and the base line between the transmitter and receiver was taken as the x axis. The coordinate system was scaled so that 1 cm corresponds to an actual distance of 250 meters. A fortran program was written based on Equation 2.10 which produces y values for 250 meter increments of the x coordinate. The equirange contour lines were manually plotted on the map for the first 22 range cells.

The limitations initially placed on the data collection area by the sponsor were that the powers from 3 to 5 range cells were to be estimated with the bistatic angle, β , held between 120° and 160° . These requirements were altered during the course of the research in that the sponsor specified three actual target sites on the aforementioned map.

3.2.2 Identifying the Antenna Patterns. Little information was available about the antenna characteristics in addition to the parabolic dish diameter and the gain of the horn antenna. However from the information available it was necessary to determine the beam widths of the main lobes and side lobes of both antennas and their locations relative to the antenna bore sight so that the clutter block area determined by the intersection of the two patterns could be determined.

3.2.2.1 *The Transmitting Antenna.* As previously stated the only information available on the transmitting antenna pattern was that the main lobe beam width was approximately 1° . In order to identify the side lobe beam width and relative locations of the side lobes as well as the gains associated with the beam widths it was necessary to perform some reverse engineering. No information was available to the researcher about the dish feed antenna or the illumination pattern.

As a first attempt to identify a feed pattern which produced a 1° beamwidth, the parabolic reflector was treated as uniformly illuminated circular aperture, where the transmitting antenna had a diameter of 8.5344 meters. Kraus (7:344) gives the normalized field pattern as:

$$E_n(\theta) = 2 \frac{J_1 \left[\left(\frac{\pi D}{\lambda} \right) \sin \theta \right]}{\left(\frac{\pi D}{\lambda} \right) \sin \theta} \quad (3.1)$$

Where:

D = the diameter of the aperture

θ = the angle with respect to the normal to the aperture

J_1 = first order Bessel function

The normalized power pattern can be obtained from Equation 3.1 as:

$$F_n(\theta) = \frac{f(\theta)}{f(\theta_{max})} = |E_n(\theta)|^2 = \left\{ 2 \frac{J_1 \left[\left(\frac{\pi D}{\lambda} \right) \sin \theta \right]}{\left(\frac{\pi D}{\lambda} \right) \sin \theta} \right\}^2 \quad (3.2)$$

The beam width for the main beams will be taken as the 3 dB beam width of the normalized antenna power patterns. The 3 dB points occur at the point where Equation 3.2 drops to a value of $1/2$ from the maximum power point which occurs on bore sight. Letting $x = \pi D / \lambda \sin \theta$, implies that:

$$\frac{J_1(x)}{x} = \frac{1}{2\sqrt{2}} \approx 0.35355 \quad (3.3)$$

Using Balanis' $J_1(x)/x$ table (1.943) and interpolating to find the value of x for $J_1(x)/x = 0.35355$ yields $x = 1.61612$. But $x = \pi D/\lambda \sin \theta$, therefore the 3 dB point occurs at $\theta = \arcsin(1.61612\lambda/\pi D)$. The half power beam width (HPBW) is equal to twice the 3 dB point, hence:

$$HPBW_{mb} = 2 \arcsin \left(\frac{1.61612\lambda}{\pi D} \right) \quad (3.4)$$

Applying Equation 3.4 to the transmitting antenna yields a beam width of 0.7° . In an attempt to locate a feed pattern which produced more acceptable results, the feed pattern was assumed to have a parabolic taper. Stutzman and Thiele (17:420-421) provide information in tabular format for several orders of parabolic taper and edge illumination. Using the HPBW as a guide it was determined that the transmitter pattern more closely matches a second order parabolic taper. They estimate the HPBW in radians as:

$$HPBW(rad) = \frac{1.47\lambda}{2a} = \frac{1.47\lambda}{D} \quad (3.5)$$

Using a wavelength of 10 cm and a dish diameter of 853.44 cm in Equation 3.5 yields a HPBW which is approximately 1° .

$$HPBW(rad) = \frac{(1.47)(10)}{853.44} = 0.0172244 rad = 0.986^\circ \quad (3.6)$$

The normalized field pattern associated with a second order parabolic taper is given by:

$$E_n(\theta) = \frac{43 J_3 \left(\frac{\pi D}{\lambda} \sin \theta \right)}{\left(\frac{\pi D}{\lambda} \sin \theta \right)^3} \quad (3.7)$$

The normalized power pattern of the antenna is equal to the square of the normalized field pattern, therefore:

$$F_n(\theta) = \left[\frac{48 J_3\left(\frac{\pi D}{\lambda} \sin \theta\right)}{\left(\frac{\pi D}{\lambda} \sin \theta\right)^3} \right]^2 \quad (3.8)$$

The location of the side lobes and the respective 3 dB down beam widths must be determined for the antenna pattern. The first side lobes occur at the first peak of the Bessel function away from bore sight. Referring the the Balanis tables again (1:942) this peak at $x \approx 7.9167$. But $x = \pi D / \lambda \sin \theta$, therefore setting the two quantities equal and rearranging to solve for θ yields the center line direction for the first side lobes.

$$\theta_{sl} = \pm \arcsin \left(\frac{7.9167 \lambda}{\pi D} \right) \quad (3.9)$$

Solving Equation 3.9 to determine the angle which corresponds to the side lobe center lines for the transmitter (θ_{slt}) yields $\theta_{slt} = 1.70^\circ$. The normalized power levels at the side lobe center lines was obtained from Equation 3.8 by setting $x = 7.9167$ and solving which yielded a power of $816.956 \mu W$ or -30.9 dB. At the 3 dB down points from the side lobe center line this power is cut in half to $408.48 \mu W$. Therefore solving for the corresponding angle $F_n(\theta) = 408.48 \mu W$ yields a recursion equation in x . Solving the equation yields $x \approx 8.81$. Replacing 7.9167 in Equation 3.9 with 8.81 and solving identifies the location of one of the 3 dB down angles.

$$\theta_{slhp} = \pm \arcsin \left(\frac{8.81 \lambda}{\pi D} \right) \quad (3.10)$$

Using Equation 3.10 to find the side lobe 3 dB down angles for the transmitter produces 1.88° . The side lobe HPBW equals twice the difference between the side lobe center line angles and the 3 dB down angles. Hence for the transmitter:

$$HPBW_{sl} = 2(\theta_{slt} - \theta_{slhp}) = 0.37^\circ \quad (3.11)$$

The final process in determining the transmitter antenna pattern was to determine the appropriate gains for the main and side lobe beam widths. Barksdale (2:1-54) identifies the directive gain function of an antenna as:

$$D_g(\theta) = G_0 F_n(\theta) \quad (3.12)$$

Where G_0 in Equation 3.12 is the maximum power gain of the antenna. Equation 3.12 has been modified to no ϕ variations since the parabolic antenna in question has antenna patterns which are symmetric in the ϕ direction. The maximum power gain of the antenna, G_0 , is equal to the efficiency of the antenna times the directivity of the antenna.

$$G_0 = e D_0 \quad (3.13)$$

The efficiency of a parabolic reflector (10:6) can be estimated as, $e = 0.55$. Kraus (7:345) identifies the directivity of an antenna as:

$$D_0 = \frac{4\pi A_p}{\lambda^2} \quad (3.14)$$

Where A_p in Equation 3.14 is the physical area of the aperture. For the parabolic reflectors the aperture area is the area of a circle of diameter D . Substituting $A_p = \pi(\frac{D}{2})^2$ into Equation 3.14 results in:

$$D_0 = \left(\frac{\pi D}{\lambda}\right)^2 \quad (3.15)$$

Combining Equation 3.15 and the efficiency estimate of 0.55 in Equation 3.13 results in a maximum power gain of:

$$G_0 = 0.55 \left(\frac{\pi D}{\lambda}\right)^2 \quad (3.16)$$

Applying Equation 3.16 to the transmitting antenna in this bistatic system yields a maximum gain for the transmitter of:

$$G_0 = (0.55) \left(\frac{\pi 8.5344}{0.1} \right)^2 = 39537.4 = 45.97 \text{ dB} \quad (3.17)$$

Applying the results of Equation 3.17 to Equation 3.12 results in gain functions which can be used to identify the gains associated with the main and side lobe beam widths of the antenna. The gain of the antenna main beam was taken to be equal to the maximum directive gain. The gain for the side lobe beam widths were calculated as the gain at the side lobe center angles, $\theta = \theta_{sl} = 1.70^\circ$.

$$D_{sl}(\theta) = G_0 F_n(\theta) |_{\theta=\theta_{sl}} = 34.43 = 15.37 \text{ dB} \quad (3.18)$$

3.2.2.2 The Receiving Antenna As previously mentioned the only information provided was that the receiving antenna was a 20 dB standard gain horn antenna. From the literature reviewed the term *standard gain* was most often applied to pyramidal horn antennas designed for optimum gain. Though this was not explicitly stated in the material, the following procedures are based on this assumption.

Stutzman and Thiele (17:411-415) outline a procedure for designing an optimum gain pyramidal horn. The results of their design procedure are the pertinent physical dimensions of the antenna. These dimensions are illustrated in Figure 3.1. From these dimensions the gains and beam widths can be estimated from the universal radiation patterns provided (17:409).

From the conditions for optimum gain of E-plane and H-plane sectoral horns, Stutzman and Thiele (17:413) develop a recursion formula for designing an optimum gain pyramidal horn illustrated in Equation 3.19.

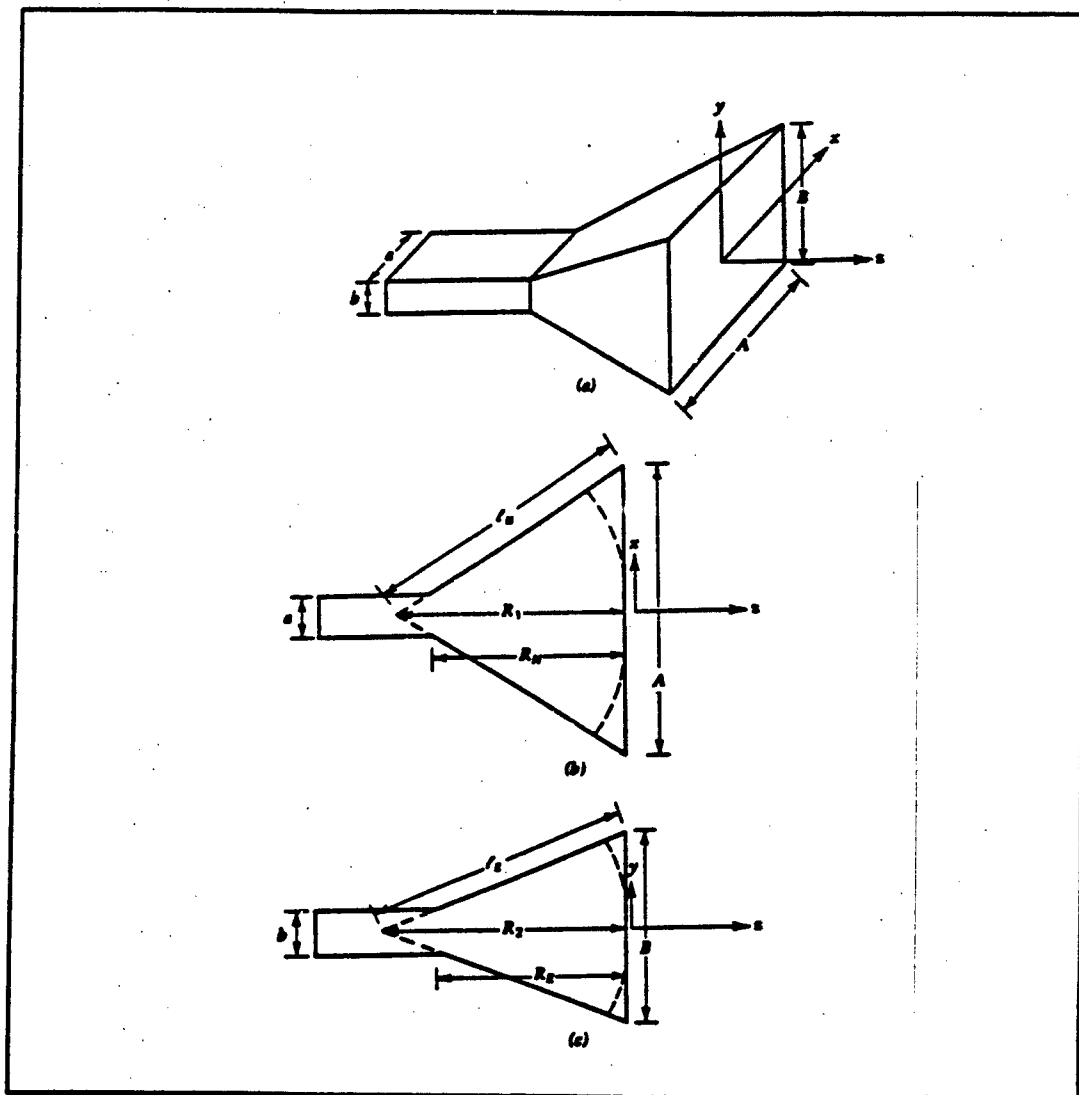


Figure 3.1. Pyramidal Horn Geometry.

$$\left[\sqrt{2\sigma} - \frac{b}{\lambda} \right]^2 (2\sigma - 1) = \left(\frac{G}{2\sqrt{2\sigma}\pi} - \frac{a}{\lambda} \right)^2 \left(\frac{G^2}{18\pi^2\sigma} - 1 \right) \quad (3.19)$$

Equation 3.19 can be used to solve for σ provided the waveguide dimensions a and b feeding the horn and the gain G are known. In Equation 3.19 σ is given by:

$$\sigma = \frac{\ell_E}{\lambda} \quad (3.20)$$

Therefore Equation 3.19 can be used to solve for σ which in turn can be used to determine the dimension ℓ_E . With the value of ℓ_E Equation 3.21 can be used to determine B .

$$B = \sqrt{2\lambda R_2} \approx \sqrt{2\lambda \ell_E} \quad (3.21)$$

With a value for B Equation 3.22 can be used to determine A .

$$G = \epsilon_{ap} \frac{4\pi}{\lambda^2} A_p = \frac{2\pi}{\lambda^2} (AB) \quad (3.22)$$

Where ϵ_{ap} in Equation 3.22 is the aperture efficiency of the antenna. An aperture efficiency of 0.5 is a common value used for horn antennas. The quantity A_p in Equation 3.22 represents the physical area of the antenna aperture which is equal to the product AB . With the lengths A and B established, the universal radiation patterns provided by Stutzman and Thiele (17:409) can then be used to identify the beam widths of the main and side lobes for both the E-plane and H-plane sectors as well as the respective directions of the side lobes relative to bore site.

The waveguide dimensions were obtained from Pozar (11:716), where he identifies a WR-284 waveguide as an appropriate choice for S band. The dimensions for WR-284 are $a = 7.214$ cm and $b = 3.404$ cm. Stutzman and Thiele suggest

an initial value of $\sigma = G/2\pi\sqrt{6}$. After many iterations, it was determined that $\sigma \approx 6.21430022$. Using this value in Equation 3.20 and solving for ℓ yields:

$$\ell = \lambda\sigma = (.1)(6.21430022) \approx 62.413\text{cm} \quad (3.23)$$

Using this result in Equation 3.21 to solve for B yields:

$$B \approx \sqrt{2\lambda\ell} = \sqrt{(2)(10)(62.413)} = 35.33\text{cm} \quad (3.24)$$

Using this value for B in Equation 3.22 and solving for A yields:

$$A = \frac{G\lambda^2}{2\pi B} = \frac{(100)(10)^2}{(2)(35.33)\pi} = 45.09\text{cm} \quad (3.25)$$

Using these values and the universal radiation patterns (17:404,409) the necessary patterns were identified. In the E-plane, the 3 dB beam width was established as 14.14° . The first side lobe occurs at 23.6° has a beam width of $7.6'$ and is 9.1 dB down from the main lobe. In the H-plane, the 3 dB beam width was established as 11.1° and the side lobes are not distinguishable from the main beam.

3.2.3 Identifying the Clutter Cells. The clutter cells assume the shape outlined by the intersection of a selected range cells, the transmitter antenna patterns, and receiver antenna patterns. Before the antenna patterns from Section 3.2.2 can be overlaid on the equirange contour lines which delineate a specific range cell, the bistatic angle for the system must be selected. As previously mentioned, the requirements were altered by the sponsor during the course of the research. Originally three bistatic angles were to be selected between 120° and 160° . In light of the fact that an adequate shadowing function had not been developed and use of a shadowing function would require digitalization of all terrain heights between the transmitter

and target as well as between the receiver and target, three sites were jointly selected by the researcher and the sponsor.

Site one was a hilly forested area located approximately 500 meters south of Lincoln, Massachusetts. The distance from site one to the transmitter (D_T) was measured to be 14.4625 Km. The distance from site one to the receiver (D_R) was measured to be 5.775 Km. The bistatic angle was determined by applying the law of cosines to the geometry involved. The general form is provided in Equation 3.26. Applying the values for D_T , D_R , and the baseline distance between the transmitter and receiver ($D_B = 19.248 \text{ Km}$) to Equation 3.26 yielded a bistatic angle of 140.0° for site one.

$$\beta = \arccos \frac{D_R^2 + D_T^2 - D_B^2}{2D_R D_T} \quad (3.26)$$

Site two was Fairhaven Hill located approximately 2.5 Km south of Concord Massachusetts. The distance from site two to the transmitter (D_T) was measured to be 11.050 Km. The distance from site two to the receiver (D_R) was measured to be 9.875 Km. Using these values in Equation 3.26 resulted in a bistatic angle of 133.7° for the physical layout of site two.

Site three was Pine Hill located approximately 500 meters west of the Hanscom Air Force Base runways. The distance from site one to the transmitter (D_T) was measured to be 16.1125 Km. The distance from site one to the receiver (D_R) was measured to be 9.9625 Km. Substituting these values into Equation 3.26 yielded a bistatic angle for site three of approximately 92.1° , which is outside of the original target range for bistatic angles.

The antenna patterns were then manually plotted on the topographic map at each of the selected sites. The intersection of the transmit and receive antenna patterns was used to identify the portions of range cells illuminated at each site. This intersection of the transmit and receive antenna patterns along with the range

cell constitutes a clutter cell. At site one, the transmit antenna's main lobe and side lobe patterns intersect with the receive antenna's main lobe pattern over range cells 3, 4, 5, and 6. The receiver antenna side lobe pattern intersects with the transmit antenna's main and side lobe patterns over range cells 6, 7, 8, and 9.

For site two, the transmit main and side lobes intersect with the receive main lobe over range cells 4, 5, 6, 7, and 8. The receive antenna side lobe intersects the transmit antenna's main and side lobes over range cells 10, 11, 12, 13, 14, and 15. As the bistatic angle decreases, the antenna pattern intersection points occur at distances farther from the baseline between the transmitter and receiver. As the intersections occur farther from the baseline, the range cells get progressively narrower and hence more range cells are illuminated.

For site three, the transmit main and side lobes intersect with the receive main lobe over range cells 18, 19, 20, 21, 22, 23, 24, 25, 26, 27, 28, and 29. The receive side lobe intersects with the transmit main and side lobes over many range cells starting from cell number 24 and continuing off the map.

In order to apply Barrick's rough surface scattering formulas, it was necessary to characterize the terrain being illuminated in the clutter cells statistically. The terrain to be characterized was first divided into rectangular blocks as shown in Figure 3.3 such that each block covers an area of terrain with homogeneous characteristics. Unfortunately, nature rarely simplifies the procedure by allowing an entire area illuminated to be composed of a single area of homogeneous characteristics. An example at this point may be helpful.

Assume that a particular clutter cell has been identified on the topographic map. The terrain area of the cell is partially composed of forested hills and partially composed of rolling grass land. The site would have to be divided into two rectangular blocks, one to characterize the forested area and a second to characterize the grass land. The intersection of the clutter cell and the forested characterization block would be considered a clutter block. Similarly, the intersection of the grass land

characterization block and the clutter cell would comprise a second clutter block. To find the scattered power from this section of the range cell would require solving for the clutter power from each clutter block individually. The total power from the two clutter blocks would be the sum of the individual magnitudes.

3.3 Terrain Site Characterization.

It is easy to see how performing these calculations manually could quickly become an accounting nightmare. The area illuminated by the receive antenna main lobes and the transmitter antenna's total pattern covers portions of five range cells. The receive antenna's side lobes intersect with the transmitter antenna's full pattern over portions of six range cells. In this situation, each range cell is composed of from one to three clutter cells. The complexity increases with the number of clutter blocks involved with each clutter cell. For these reasons, only three range cells at each site were selected for the demonstration of the process described in Chapter two.

Several pieces of statistical information from each homogeneous terrain area to be characterized were required to apply Barrick's formulas for determining the NRCS of the areas in question.

First, recall from Section 2.4.3 that knowledge of the height distribution was required to solve the surface current integral in Equation 2.41. In this research, the distribution has been assumed to be a joint Gaussian probability density function denoted by the random variable $\zeta(X, Y)$. One advantage to this assumption is that Barrick (13:721) has provided a closed form solution for Equation 2.41 when the distribution is Gaussian.

Barrick also provides a closed form solution for a joint exponential height distribution (13:721) however, Roseman (12:1-2) disputes the validity of the joint exponential distribution as a valid joint probability distribution function and raises questions as to its validity for representing rough surfaces. Therefore, for any distri-

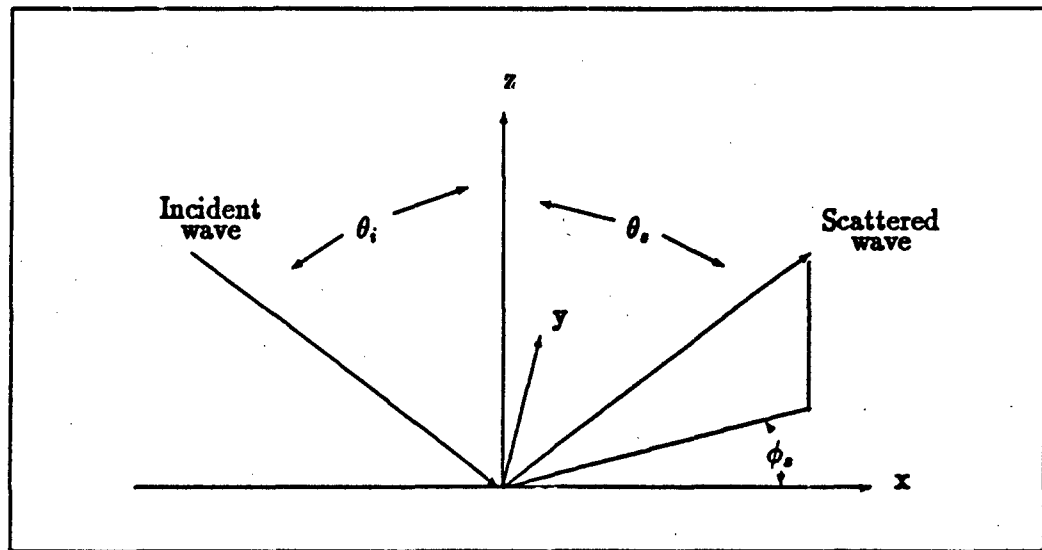


Figure 3.2. Terrain Scattering Geometry.

bution other than the joint Gaussian pdf, Equation 2.41 would probably have to be solved numerically.

Second, the reference plane depicted in Figure 3.2 is co-planer with a plane passing through the mean value of the surface height distribution. Therefore, the sample mean of the random variable $\zeta(X, Y)$ was required to determine the incident angle and scattering angles of the electromagnetic energy at the terrain site.

The third statistical quantity required from the surface height distribution was the sample variance of the surface heights. The quantity was used directly in Barrick's closed form solution of Equation 2.41 (13:721). Barrick refers to the variance of the sample mean as the mean square roughness height and identifies it with the symbol h^2 .

The final data, and probably the most difficult information to estimate, is the correlation length of the joint Gaussian distribution.

With the knowledge of these four items, Barrick's formulation can be used to determine a value of NRCS for the terrain area covered by the statistical distri-

bution. Once the NRCS was known, the RCS of that portion of the terrain visible simultaneously to both antennas was easily calculated.

The terrain areas to be characterized were divided into rectangular areas with homogeneous characteristics as shown in Figure 3.3. The total area was divided along each axis into n blocks of width δ_r . The result was n^2 blocks each with an area of δ_r^2 square meters.

The terrain height at any point in the area depicted in Figure 3.3 was treated as a random variable denoted by $\zeta(X, Y)$. The distribution of the surface heights represented by $\zeta(X, Y)$ was assumed to be jointly Gaussian. This is a valid assumption by the central limit theorem as long as the value of n is kept large to provide a large number of sample points (n^2). For the central limit theorem to be appropriate, the sample mean and variance must not approach extreme values.

Each block in the characterization area was in turn treated as a random variable, $\zeta(X = i\delta_r, Y = j\delta_r)$, which was also assumed to represent a joint Gaussian distribution of heights. If the Gaussian assumption was not made, each of the blocks in Figure 3.3 would have to be sampled at increments small enough to allow accurate development of the governing probability distribution for each block.

This procedure would become almost impossible when working from a topographic map because of the various sizes of the homogeneous areas to be characterized. The size of the homogeneous areas can vary from several square Kilometers down to several hundred square meters. Unfortunately, the contour lines are only placed at three meter height intervals and for small characterization areas the distributions for the individual blocks would appear as uniform distributions at a single height. Except for a limited number of cases, this would probably be a misleading characterization of the height distributions.

One can extract useful information about the properties of the $n^2 \zeta(i, j)$ distributions based on the assumption that they are all Gaussian, the characteristics of

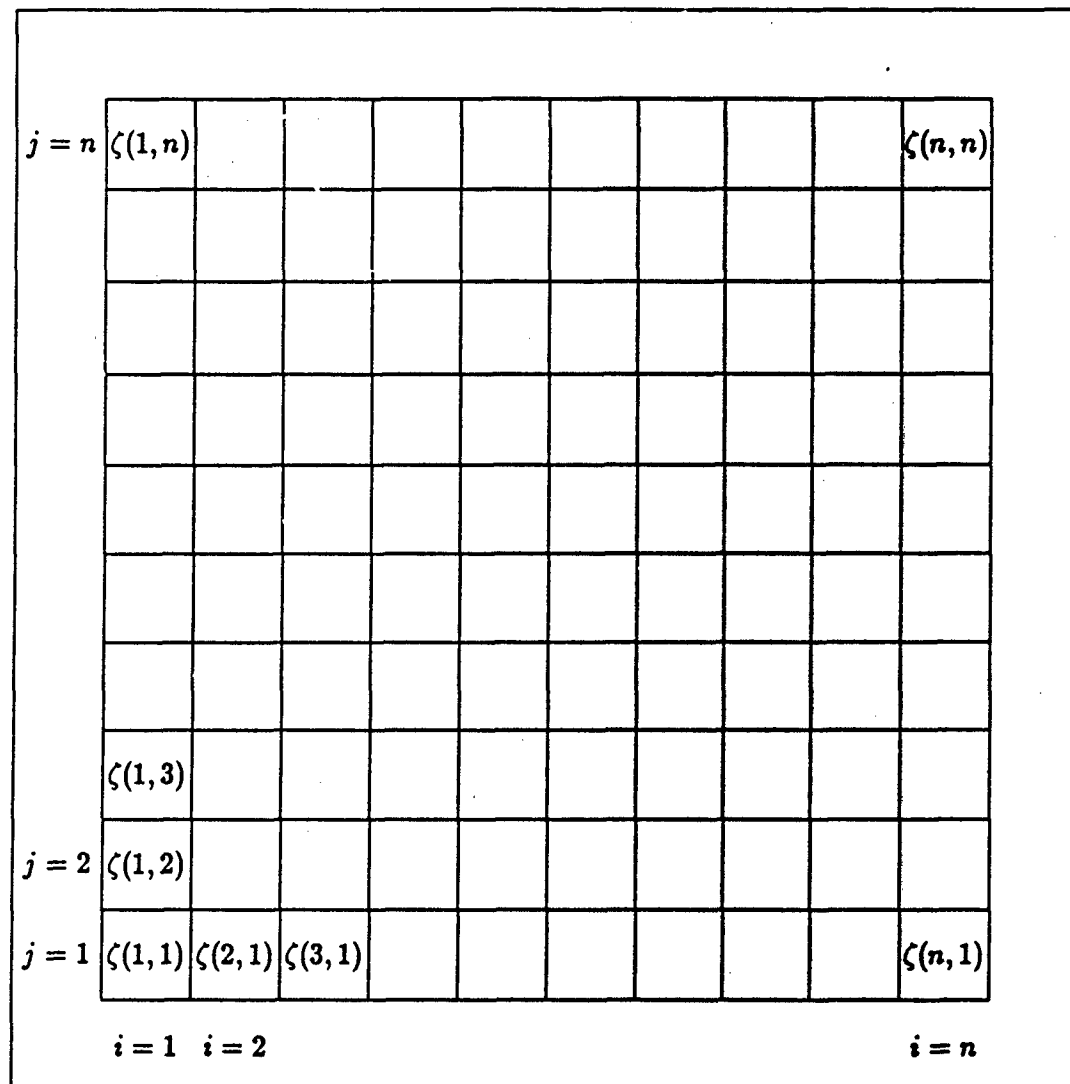


Figure 3.3. Terrain Site Characterization Geometry.

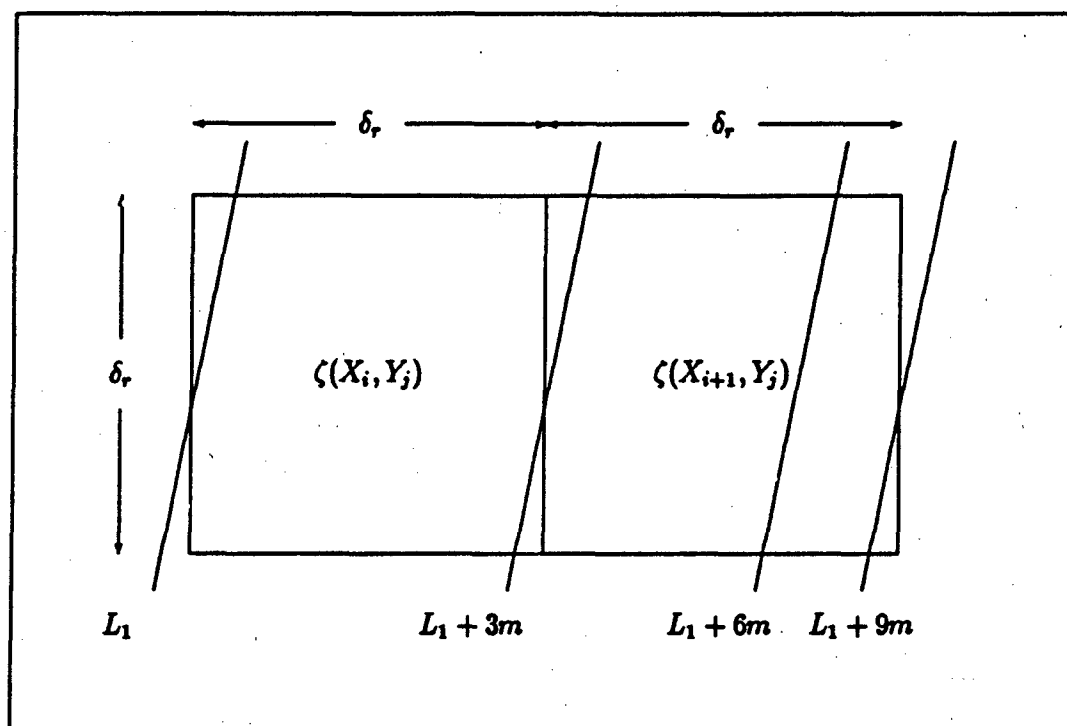


Figure 3.4. Determining the Sample Point Mean from Contour Lines.

the information provided by the contour lines of the topographic map, and proper selection of the spacing δ_r .

3.3.1 Determining the Sample Point Mean Value. As previously mentioned, the contour lines on the USGS topographic map are labeled at intervals of three meters. The size of the areas represented by the $n^2 \zeta(i, j)$ distributions is determined by the selection of the quantity δ_r . If δ_r is selected such that a majority of these distribution areas coincide within the area delimited by two contour lines, a reasonable estimate of the mean value of the individual distributions can be extracted. Figure 3.4 is provided to illustrate this point.

Figure 3.4 illustrates two distribution areas labeled $\zeta(i, j)$ and $\zeta(i + 1, j)$. The distribution area identified as $\zeta(i, j)$ is bounded by two contour lines labeled L_1 and

L_{1+3m} . From this one can infer that a majority of the surface heights in $\zeta(i, j)$ must lie between the two values represented by the contour lines. In this case, the mean value of $\zeta(i, j)$ would be determined by:

$$\mu_{i,j} = \frac{L_{1+3m} - L_1}{2} + L_1 \quad (3.27)$$

Even if great care is taken in selecting the proper value of δ_r , there will still be distribution areas which engulf more than two contour lines. This is illustrated by the distribution area labeled $\zeta(i + 1, j)$ in Figure 3.4. The concept described by Equation 3.27 can easily be extended to include the multiple contour line case as:

$$\mu_{i,j} = \frac{L_h - L_l}{2} + L_l \quad (3.28)$$

Where:

L_h represents the contour line of highest value.

L_l represents the contour line of lowest value.

Applying Equation 3.28 to the distribution area in Figure 3.4 which is labeled $\zeta(i + 1, j)$ would yield:

$$\mu_{i,j} = \frac{L_{1+9m} - L_{1+3}}{2} + L_{1+3m} \quad (3.29)$$

By carefully selecting the proper value for δ_r and using the procedure outlined by Equations 3.27 and 3.28 valid mean values for the n^2 blocks in each site can be identified.

3.3.2 Determining the Sample Point Variance. The variance of the distribution areas illustrated in Figure 3.4 can also be determined with reasonable accuracy from the data provided by the topographic map contour lines. Using the distribution area represented by $\zeta(i, j)$ in Figure 3.4, one can again infer that a majority of the

surface heights fall between the values identified by the contour lines labeled L_1 and L_{1+3m} . For a Gaussian distribution, 95.4 percent of the distribution values fall within plus or minus two standard deviations of the mean value. To derive the variance of a particular area, it was assumed that the difference in contour line values represented plus or minus two standard deviations.

$$4\sigma = L_1 - L_{1+3m} \quad (3.30)$$

Solving equation 3.30 for σ and noting that the variance equals the standard deviation squared yielded the following formula for distribution areas bounded by two contour lines:

$$\sigma_{i,j}^2 = \frac{(L_{1+3m} - L_1)^2}{16} \quad (3.31)$$

Extending Equation 3.31 to the cases where the distribution area was bounded by more than one contour line can be illustrated by $\zeta(i+1, j)$ in Figure 3.4. For distribution areas similar to $\zeta(i+1, j)$, the plus or minus two standard deviations is now represented by the difference in height of the highest value contour line and the lowest value contour line.

$$\sigma_{i,j}^2 = \frac{(L_h - L_l)^2}{16} \quad (3.32)$$

3.3.3 Estimating the Sample Mean and Variance. The sample mean value was estimated as the average value of the mean values of the sample point distributions. The estimate of the sample mean was determined using the following equation:

$$\hat{\mu} = \frac{1}{n^2} \sum_{i=1}^n \sum_{j=1}^n \mu_{ij} \quad (3.33)$$

In a similar manor the estimate of the sample variance was taken as the average value of the variances of the individual sample point distributions. The estimate of the sample variance was determined using the following equation:

$$\widehat{\sigma^2} = \frac{1}{n^2} \sum_{i=1}^n \sum_{j=1}^n (\mu_{ij} - \bar{\mu})^2 \quad (3.34)$$

3.3.4 Estimating the Sample Correlation Length. The correlation length is defined as the distance required to cause the correlation function reach a value of $\frac{1}{e}$. The correlation function for the joint Gaussian distribution as it applies to the problem at hand is given by:

$$\rho_{\zeta(i,j), \zeta(m,n)} = \exp \left(-\frac{r^2}{l^2} \right) \quad (3.35)$$

In Equation 3.35 $\zeta(i,j), \zeta(m,n)$ are any two of the n^2 joint Gaussian distributions which are part of $\zeta(X,Y)$. The quantity l represents the correlation length or distance between the two selected distributions. The quantity r represents the distance between the two selected distributions and is given by:

$$r^2 = (X_i - X_m)^2 + (Y_j - Y_k)^2 \quad (3.36)$$

The correlation function for any two distributions can also be expressed as:

$$\rho_{\zeta_{ij}\zeta_{mk}} = \frac{E[(\zeta_{ij} - \mu_{ij})(\zeta_{mk} - \mu_{mk})]}{\sigma_{ij}\sigma_{mk}} \quad (3.37)$$

Where in Equation 3.37 the $E[\cdot]$ represents the average or expected value of the argument. Carrying out the multiplication of terms in Equation 3.37 and using the fact that the expected value of a sum is equal to the sum of the expected values, allows the correlation function to be expressed as:

$$\rho_{\zeta_{ij}\zeta_{mk}} = \frac{E[\zeta_{ij}\zeta_{mk}] - \mu_{ij}\mu_{mk}}{\sigma_{ij}\sigma_{mk}} \quad (3.38)$$

For any given combination of sample distributions, all the quantities in Equation 3.38 can be determined with the exception of $E[\zeta_{ij}\zeta_{mk}]$. Similarly for any combination of surface distributions, the only unknown quantity in Equation 3.37 is the correlation distance. By equating the two equations and determining an estimate for $E[\zeta_{ij}\zeta_{mk}]$ an average value for the correlation distance could be determined.

During the literature search, the researcher could find no accurate method described to estimate $E[\zeta_{ij}\zeta_{mk}]$. It effectively represents how much inter-dependence there is between two surface heights in this problem. It was decided to estimate $E[\zeta_{ij}\zeta_{mk}]$ by the variance estimator for the sample $\widehat{\sigma^2}$. Making this substitution into Equation 3.38 and equating Equations 3.37 and 3.38 yields:

$$\exp\left(-\frac{r^2}{l^2}\right) = \frac{\widehat{\sigma^2} - \mu_{ij}\mu_{mk}}{\sigma_{ij}\sigma_{mk}} \quad (3.39)$$

Taking the logarithm of both sides of Equation 3.39 and solving for l^2 produces the following expression:

$$l^2 = \frac{r^2}{\ln\left(\frac{\widehat{\sigma^2} - \mu_{ij}\mu_{mk}}{\sigma_{ij}\sigma_{mk}}\right)} \quad (3.40)$$

Equation 3.40 provides a value for the correlation distance for a single combination of surface height distributions. However, any individual distribution could be correlated with any of the other distributions. Since there are n^2 distributions, there are n^4 possible combinations of distributions. With this in mind, the estimator for the average correlation distance is provided below.

$$\hat{r}^2 = \frac{1}{n^4} \sum_{i=1}^n \sum_{j=1}^n \sum_{m=1}^n \sum_{k=1}^n \frac{r^2}{\ln \left(\frac{\hat{\sigma}^2 - \mu_{ij} \mu_{mk}}{\sigma_{ij} \sigma_{mk}} \right)} \quad (3.41)$$

Where r^2 in Equation 3.41 is given by Equation 3.36. A FORTRAN program titled *SiteChar.for* was developed to determine the estimators previously described (\hat{r}^2 , $\hat{\sigma}^2$, and $\hat{\mu}$) from the site data which was manually extracted from the topographic map.

3.4 Determining the NRCS of the Site Characterization Block.

At this point in the process, the topographic map has been annotated at each of the selected sites with the range cell lines and the antenna patterns for both the transmitter and receiver. To apply the concepts outlined in the previous sections the raw data must be extracted from the map at each site. A single homogeneous area at each site was selected for analysis. From each of these areas three range cells were selected.

The range cells selected for site one were cell numbers three, four, and five. At site two, range cell numbers five, six, and seven were selected. Finally at site three, range cell numbers 21, 22, and 23 were selected for the calculations that follow.

The areas to be characterized were too small to allow the data to be directly extracted from the map. Therefore, the selected areas of the three map sites were enlarged via photocopier to allow more accurate data extraction. The three areas received different degrees of enlargement due to the varying density of the contour lines at each site.

The characterization blocks used were divided into 400 equally spaced areas. The value of 400 was selected to insure enough sample points were used to insure the assumption that the random variable, $\zeta(X, Y)$, was jointly Gaussian. The assumption was based on the central limit theorem which requires a large number of samples. A more realistic picture of the distribution would be possible with even

more sample points however, all data points had to be extracted from the map by hand. The value of 400 sub areas was a compromise to minimize the manual labor required to extract data at each site and still maintain the validity of the Gaussian assumption which was based on the central limit theorem.

Site one was divided into 400 square sub areas which measured 23.348 m per side. The total area encompassed by the site one characterization area was 218.052 Km^2 . Each of the sub areas in site two were 31.667 m per side. The total area involved for site two was 401.12 Km^2 . Finally, the sub areas in site three were 37.703 m per side for a total area of 568.61 Km^2 .

The input data to the FORTRAN program *Sitechar.for* took the form of two real numbers per sub area. The first number represented the value of the highest contour line bordering the area and the second number represented the lowest value contour line bordering the area. With these inputs, *Sitechar.for* calculated the mean ($\hat{\mu}$), the variance ($\hat{\sigma}^2$), and the correlation length (l) estimates for the sample. Table 3.1 displays the results of running the program *Sitechar.for* on the three sets of input data. All of the collected and calculated data is provided in appendix A.

3.5 Calculating the Range Cell Power.

The clutter power from each range cell was calculated with Equation 2.25 for each range cell at both polarizations. Before Equation 2.25 could be utilized the NRCS for each site characterization area had to be determined. A second FORTRAN program titled *Sigma.for* was written to determine the NRCS from the site characterization data and knowledge of the locations of the site, transmitter, and receiver.

Once the NRCS for the characterization area was know, the clutter block areas were determined and used along with the known antenna gains to determine the clutter power from each block. Summing the clutter power from all blocks located within a range cell yielded the total clutter power from the range cell in question.

| | Site 1 | Site 2 | Site 3 |
|----------------------|-----------------------|-----------------------|-----------------------|
| δ_r | 23.348m | 31.667m | 37.703m |
| $\hat{\mu}$ | 81.859m | 73.748m | 44.084m |
| $\widehat{\sigma^2}$ | 186.074m ² | 209.830m ² | 68.574m ² |
| ρ^2 | 45.687m ² | 82.365m ² | 116.587m ² |

Table 3.1. Site Characterization Data.

| | Site 1 | Site 2 | Site 3 |
|-----------------|----------|----------|--------|
| σ_{hh}^o | 2.539277 | 3.262236 | 0.0 |
| σ_{vv}^o | 71.11379 | 326.910 | 0.0 |

Table 3.2. NRCS Data from *Sigma.for*.

The output from the program *Sigma.for* was two NRCS values for the characterization area. The first for both transmitter and receiver using vertical polarization and the second for both employing horizontal polarization. The input files used and the data files resulting from *Sigma.for* were included in Appendix A. Table 3.2 lists the results of running the program.

The input data required for *Sigma.for* included:

1. The transmitter to clutter cell distance (D_t).
2. The receiver to clutter cell distance (D_r).
3. The sample mean estimate ($\hat{\mu}$).
4. The sample variance estimate ($\hat{\sigma}^2$).
5. The relative permittivity of the site characterization area (ϵ_r).
6. The transmitter site elevation (h_t).
7. The receiver site elevation (h_r).
8. The correlation length of the sample (l).

All three of the characterization sites were populated by trees and the average value for the relative permittivity was taken to be $4.0 + j0.45$ (8:8). The site areas

were assumed to be composed of non-magnetic material and the average value for the relative permeability was taken to be $1.0 + j0.0$.

3.5.1 Clutter Power for Site One. The clutter power for three range cells was determined for site one. The selected range cells were cells three, four, and five.

When using vertical polarization, three clutter blocks were illuminated by the transmitter and receiver antenna patterns. One of the blocks was created by the intersection of the two antenna main beams. The remaining two blocks were created by the intersection of the transmit antenna side lobe and the receive antenna main lobe. Inserting the known information for range cell three into Equation 2.25 yields:

$$P_c = \frac{P_t \lambda^2 G_{Rm} \sigma_{vv}}{(4\pi)^3} \left[\frac{G_{Tm} A_{c1}}{D_{t1}^2 D_{r1}^2} + \frac{G_{Ts} A_{c2}}{D_{t2}^2 D_{r2}^2} + \frac{G_{Ts} A_{c3}}{D_{t3}^2 D_{r3}^2} \right] \quad (3.42)$$

Where:

G_{Tm} = The transmit antenna main lobe gain (39537.4).

G_{Ts} = The transmit antenna side lobe gain (34.43).

G_{Rm} = The receive antenna main lobe gain (100.0).

A_{C1} = The area outlined by the intersection of both antenna main beams and the equirange contour lines which define range cell 3 ($200000m^2$).

A_{C2} = The first area outlined by the transmit antenna side lobe, the receive antenna main lobe, and the equirange contour lines which define range cell 3 ($65390m^2$).

A_{C3} = The second area outlined by the transmit antenna side lobe, the receive antenna main lobe and equirange contour lines which define range cell 3 ($287500m^2$).

D_{t1} Was the distance from the center of the first clutter block (A_{C1}) to the transmitter (13450 m).

D_{t2} Was the distance from the center of the second clutter block (A_{C2}) to the transmitter (12650 m).

D_{t3} Was the distance from the center of the third clutter block (A_{C3}) to the transmitter (14425 m).

D_{r1} Was the distance from the center of the first clutter block (A_{C1}) to the receiver (6550 m).

D_{r2} Was the distance from the center of the second clutter block (A_{C2}) to the receiver (7350 m).

D_{r3} Was the distance from the center of the third clutter block (A_{C3}) to the receiver (5575 m).

σ^0 = The NRCS for the site one characterization area (71.11379).

Substituting these values into Equation 3.42 and performing the indicated operations yielded a received clutter power of 30.209 mW for range cell three using vertical polarization.

For the case of both receiver and receiver using horizontal polarization, range cell three contains only two clutter blocks. The first was defined by the intersection of the antenna main beams and had an area of $109375m^2$. The second clutter block was defined by the intersection of the transmit antenna side lobe and the receive antenna main lobe and had an area of $220000m^2$. Using these value in Equation 3.42 along with $\sigma_{AA} = 2.621544$ yielded a clutter power of 5.900 mW.

All of the range cells for all three sites could be calculated with Equation 3.42. In some instances, one of the clutter blocks defined by the intersection of the transmit antenna side lobe and the receive antenna main lobe did not fall within a particular range cell. The tables which follow summarize the pertinent range, area measurements, distances, and resulting clutter powers.

Table 3.3 provides a tabular listing of the clutter block areas, transmitter to target and receiver to target distances for both systems operating with vertical polarization. In all the range and data tables, the symbols should be interpreted as defined in Equation 3.42.

| Site 1 Vert. Pol. | Range Cell 3 | Range Cell 4 | Range Cell 5 |
|-------------------|-----------------------|-----------------------|-----------------------|
| A_{C1} | 200,000m ² | 296,875m ² | 68,750m ² |
| D_{t1} | 13,450m | 14,500m | 15,225m |
| D_{r1} | 6,550m | 5,750m | 5,275m |
| A_{C2} | 65,390m ² | 236,250m ² | 150,938m ² |
| D_{t2} | 12,650m | 13,450m | 14,625m |
| D_{r2} | 7,350m | 6,800m | 5,875m |
| A_{C3} | 287,500m ² | 134,400m ² | 0.0m ² |
| D_{t3} | 14,425m | 15,450m | N/A |
| D_{r3} | 5,575m | 4,800m | N/A |

Table 3.3. Site One Area and Range Data for Vertical Polarization.

| Site 1 Vert. Pol. | Range Cell 3 | Range Cell 4 | Range Cell 5 |
|-------------------|----------------|----------------|----------------|
| A_{C1} | 29.210mW | 48.409mW | 12.082mW |
| A_{C2} | 7.466 μ W | 27.878 μ W | 20.181 μ W |
| A_{C3} | 43.880 μ W | 24.122 μ W | 0.0mW |
| Total | 29.261mW | 48.461mW | 12.102mW |

Table 3.4. Site One Clutter Block Power, Vertical Polarization.

Table 3.4 provides the calculated clutter block powers for site one with both transmitter and receiver operating with vertical polarization.

Table 3.5 provides a tabular listing of the clutter block areas, transmitter to target and receiver to target distances for both systems operating with vertical polarization. In all the range and data tables, the symbols should be interpreted as defined in Equation 3.42.

Table 3.6 provides the calculated clutter block powers for site one with both transmitter and receiver operating with horizontal polarization.

The validity of these range cell clutter powers is unknown because the sponsor was unable to supply actual system measurements of site one.

| Site 1 Horz. Pol. | Range Cell 3 | Range Cell 4 | Range Cell 5 |
|-------------------|--------------|--------------|--------------|
| A_{C1} | $109,375m^2$ | $296,875m^2$ | $24,062m^2$ |
| D_{t1} | $13,450m$ | $14,500m$ | $15,225m$ |
| D_{r1} | $6,550m$ | $5,750m$ | $5,275m$ |
| A_{C2} | $0.0m^2$ | $196,875m^2$ | $103,125m^2$ |
| D_{t2} | N/A | $13,450m$ | $14,625m$ |
| D_{r2} | N/A | $6,800m$ | $5,875m$ |
| A_{C3} | $220,000m^2$ | $100,000m^2$ | $0.0m^2$ |
| D_{t3} | $14,425m$ | $15,450m$ | N/A |
| D_{r3} | $5,575m$ | $4,800m$ | N/A |

Table 3.5. Site One Area and Range Data for Horizontal Polarization.

| Site 1 Horz. Pol. | Range Cell 3 | Range Cell 4 | Range Cell 5 |
|-------------------|----------------|--------------|----------------|
| A_{C1} | $570.387\mu W$ | $1.729mW$ | $150.994\mu W$ |
| A_{C2} | $0.0mW$ | $829.537nW$ | $492.339nW$ |
| A_{C3} | $1.199\mu W$ | $640.867nW$ | $0.0mW$ |
| Total | $571.586\mu W$ | $1.730mW$ | $151.586\mu W$ |

Table 3.6. Site One Clutter Block Power, Horizontal Polarization.

3.5.2 Clutter Power for Site Two. Table 3.7 provides a tabular listing of the clutter block areas, transmitter to target and receiver to target distances for both systems operating with vertical polarization. In all the range and data tables, the symbols should be interpreted as defined in Equation 3.42.

Table 3.8 provides the calculated clutter block powers for site two with both transmitter and receiver operating with vertical polarization.

Table 3.9 provides a tabular listing of the clutter block areas, transmitter to target and receiver to target distances for both systems operating with vertical polarization. In all the range and data tables, the symbols should be interpreted as defined in Equation 3.42.

Table 3.10 provides the calculated clutter block powers for site two with both transmitter and receiver operating with horizontal polarization.

The validity of these range cell clutter powers is unknown because the sponsor was unable to supply actual system measurements of site two.

3.5.3 Clutter Power for Site Three. Table 3.11 provides a tabular listing of the clutter block areas, transmitter to target and receiver to target distances for both systems operating with vertical polarization. In all the range and data tables, the symbols should be interpreted as defined in Equation 3.42.

Table 3.12 provides a tabular listing of the clutter block areas, transmitter to target and receiver to target distances for both systems operating with vertical polarization. In all the range and data tables, the symbols should be interpreted as defined in Equation 3.42.

Tables 3.11 and 3.12 were included for completeness. The power level calculations for site three could not be performed because the expression for the NRCS at sight three could not be determined.

| Site 2 Vert. Pol. | Range Cell 5 | Range Cell 6 | Range Cell 7 |
|-------------------|-------------------------|-------------------------|-----------------------|
| A_{C1} | 210,000m ² | 245,000m ² | 186,046m ² |
| D_{11} | 9,875m | 10,925m | 11,875m |
| D_{r1} | 10,625m | 9,825m | 8,875m |
| A_{C2} | 121,875m ² | 132,187.5m ² | 131,250m ² |
| D_{12} | 9,425m | 10,225m | 11,175m |
| D_{r2} | 11,075m | 10,525m | 9,825m |
| A_{C3} | 132,812.5m ² | 134,922m ² | 65,609m ² |
| D_{13} | 10,675m | 11,725m | 12,600m |
| D_{r3} | 9,825m | 9,025m | 8,400m |

Table 3.7. Site Two Area and Range Data for Vertical Polarization.

| site 2 Vert. Pol. | Range Cell 5 | Range Cell 6 | Range Cell 7 |
|-------------------|----------------|----------------|----------------|
| A_{C1} | 99.400mW | 110.804mW | 87.280mW |
| A_{C2} | 50.756 μ W | 51.790 μ W | 49.404 μ W |
| A_{C3} | 54.785 μ W | 54.675 μ W | 26.576 μ W |
| Total | 99.505mW | 110.911mW | 87.356mW |

Table 3.8. Site Two Clutter Block Power, Vertical Polarization.

| site 2 Horz. Pol. | Range Cell 5 | Range Cell 6 | Range Cell 7 |
|-------------------|----------------|----------------|--------------|
| A_{C1} | $159,687.5m^2$ | $245,000m^2$ | $168,750m^2$ |
| D_{t1} | $9,875m$ | $10,925m$ | $11,875m$ |
| D_{r1} | $10,625m$ | $9,825m$ | $8,875m$ |
| A_{C2} | $46,094m^2$ | $132,187.5m^2$ | $131,250m^2$ |
| D_{t2} | $9,425m$ | $10,225m$ | $11,175m$ |
| D_{r2} | $11,075m$ | $10,525m$ | $9,825m$ |
| A_{C3} | $132,812.5m^2$ | $134,922m^2$ | $37,500m^2$ |
| D_{t3} | $10,675m$ | $11,725m$ | $12,600m$ |
| D_{r3} | $9,825m$ | $9,025m$ | $8,400m$ |

Table 3.9. Site Two Area and Range Data for Horizontal Polarization.

| site 2 Horz. Pol. | Range Cell 5 | Range Cell 6 | Range Cell 7 |
|-------------------|----------------|--------------|----------------|
| A_{C1} | $754.263\mu W$ | $1.106mW$ | $799.994\mu W$ |
| A_{C2} | $191.560nW$ | $516.812nW$ | $493.006nW$ |
| A_{C3} | $546.702nW$ | $545.601nW$ | $151.581nW$ |
| Total | $755.001\mu W$ | $1.107mW$ | $800.639\mu W$ |

Table 3.10. Site Two Clutter Block Power, Horizontal Polarization.

| Site 3 Vert. Pol. | Range Cell 21 | Range Cell 22 | Range Cell 23 |
|-------------------|---------------|---------------|---------------|
| A_{C1} | $97,500m^2$ | $97,500m^2$ | $97,500m^2$ |
| D_{11} | $15,325m$ | $15,625m$ | $15,950m$ |
| D_{r1} | $9,925m$ | $9,850m$ | $9,800m$ |
| A_{C2} | $35,000m^2$ | $64,471.4m^2$ | $65,000m^2$ |
| D_{12} | $14,825m$ | $15,150m$ | $15,450m$ |
| D_{r2} | $10,425m$ | $10,350m$ | $10,300m$ |
| A_{C3} | $69,062.5m^2$ | $69,062.5m^2$ | $69,062.5m^2$ |
| D_{13} | $15,850m$ | $16,150m$ | $16,475m$ |
| D_{r3} | $9,400m$ | $9,350m$ | $9,275m$ |

Table 3.11. Site Three Area and Range Data for Vertical Polarization.

| Site 3 Horz. Pol. | Range Cell 21 | Range Cell 22 | Range Cell 23 |
|-------------------|---------------|---------------|---------------|
| A_{C1} | $97,500m^2$ | $97,500m^2$ | $97,500m^2$ |
| D_{t1} | $15,325m$ | $15,625m$ | $15,950m$ |
| D_{r1} | $9,925m$ | $9,850m$ | $9,800m$ |
| A_{C2} | $937.5m^2$ | $52,500m^2$ | $65,000m^2$ |
| D_{t2} | $14,825m$ | $15,150m$ | $15,450m$ |
| D_{r2} | $10,425m$ | $10,350m$ | $10,300m$ |
| A_{C3} | $69,062.5m^2$ | $69,062.5m^2$ | $69,062.5m^2$ |
| D_{t3} | $15,850m$ | $16,150m$ | $16,475m$ |
| D_{r3} | $9,400m$ | $9,350m$ | $9,275m$ |

Table 3.12. Site Three Area and Range Data for Horizontal Polarization.

IV. Conclusions and Recommendations

4.1 Conclusions

It was impossible to establish how accurate the process proposed by this research was due to the lack of actual data as a source of comparison. However, the power levels calculated for the selected range cells at sites one and two were not entirely unreasonable for the transmitter power and distances involved. This in itself was a degree of success.

The research did provide some insight into the complexity of realistically implementing the process and indicated areas requiring further research. The most obvious of these areas was discovered with the site three data. Barrick's very rough surface formulation fails for the special case when dealing with the combination of low grazing angles and a bistatic angle which approaches 90° .

Recall from Chapter 2 the NRCS was determined from the expression:

$$\gamma_{pq} = |\beta_{pq}|^2 J \quad (4.1)$$

Where in Equation 4.1, β_{pq} represents a modified scattering matrix element and the J term the field component. For the Joint Gaussian distribution, J was given by:

$$J = \frac{4}{s^2 \xi_z^2} \exp \left[-\frac{1}{s^2} \left(\frac{\xi_x^2 + \xi_y^2}{\xi_z^2} \right) \right] \quad (4.2)$$

Where the quantities in Equation 4.2 s^2 , ξ_x , ξ_y , and ξ_z have been defined as:

$$\xi_x = \sin \theta_i - \sin \theta_s \cos \phi_s \quad (4.3)$$

$$\xi_y = \sin \theta_i \sin \phi_s \quad (4.4)$$

$$\xi_z = -\cos \theta_i - \cos \phi_s \quad (4.5)$$

At low grazing angles, ($\theta_g < 5^\circ$ where θ_g has been defined as $\frac{\pi}{2} - \theta_i$), the exponential argument blossoms rapidly. This is due to the ξ_z^2 in the denominator of the exponent's argument. For small values of θ_i , θ_g approaches $\frac{\pi}{2}$ and hence the cosine of θ_g approaches zero. Similarly, as the bistatic angle approaches $\frac{\pi}{2}$ so does θ_s . When the two situations occur simultaneously, ξ_z^2 rapidly approaches zero and renders the calculation of questionable value.

A second complication with the process was the actual data extraction from the topographic map. The process was extremely time consuming when performed manually. For the three sites in the project, it took approximately twelve hours to extract the data and enter it into a data base. For the process to realistically be used, the entire target area would have to be characterized which in turn implies extracting data from the map for the entire radar coverage area.

The process was unable to include the effects of small scale roughness on the received clutter power due to the lack of detailed information on the terrain population. It is unknown what the magnitude of this contribution could amount to. If it is not a significant contributor to the over all range cell clutter power, the costs of collecting adequate data to establish its level may far exceed the return.

Finally, at low grazing angles, a shadowing function is almost imperative. The problem again is that the shadowing function is of little use without knowledge of all the terrain between the transmitter, receiver, and target.

4.2 Recommendations

The first priority would be to establish the relative validity of the clutter powers by direct comparison with measured values. This would be a much more efficient process if the hardware were located AFIT where the researched has access to it.

Manually extracting topographic data has a prohibitive man hour cost. The collection of height data for the very rough surface scattering must be automated. One possible approach to this end would be the use of DTED data. However, the digitized data comes in a half inch tape format and requires a relatively long lead time to acquire.

If digital site data were available, the homogeneous terrain areas could be used to establish their probability distribution on an area by area basis. This would also require new solutions to the radiation integral in Chapter 2 which establishes a value for J . The automated data could also be useful for establishing the validity of the Gaussian height distribution assumption which was based solely on the loose interpretation of the central limit theorem.

Appendix A. *Software*

The following FORTRAN program titled *Sitechar.for*, was used to calculate the sample mean, variance, and correlation length estimators.

The input data files consisted of n^2 sets of numbers which represented the highest contour line value and the lowest contour line value which delimited each sub area in the sample. The three input data files (Site1.dat, Site2.dat, and Site3.dat) are included in Appendix B. The results of the computations are included in three data files (Site1prb.dat, Site2prb.dat, and Site3prb.dat ; which are also provided in Appendix B.

```

c
c
c
C
c
SITECHAR.FOR
c
c
IMPLICIT NONE
C
C
variable declarations
C
integer          i           ! loop index
integer          j           ! loop index
integer          n           ! loop index
integer          m           ! loop index
real*8           logarg
real*8           high        ! upper contour line

```

| | | |
|--------------|----------------|------------------------------|
| real*8 | low | ! lower contour line |
| real*8 | nsamp | ! number of samples per axis |
| real*8 | mu | ! mean estimator |
| real*8 | rsqrd | ! distance between dist |
| real*8 | hsqrd | ! variance estimator |
| real*8 | lsqrd | ! correlation length est |
| real*8 | delr | ! sample separation distanc |
| real*8 | zeta(500,500) | ! mu Z(i,j) |
| real*8 | sigma(500,500) | ! standard deviation Z(i,j) |
| real*8 | treg | ! temp storage reg |
| character*15 | infilnam | ! file with height samps |
| character*15 | outfilnam | ! file with results |

C

C

initialize variables

C

| | |
|------------|----------------------------|
| nsamp=20.0 | ! set to number of samples |
| delr=10.0 | ! sample sep distance |
| hsqrd=0.0 | |
| mu=0.0 | |
| lsqrd=0.0 | |

C

C

get input data file name

C

write(*,440)' Enter input data file name :'
read(*,450) infilnam

C

C

get output file name

C

```

write(*,440)' Enter output data file name:'
read(*,450) outfilnam

C
C
C
get number divisions per axis

write(*,440)' Enter number of divisions per axis:'
read(*,480)nsamp

C
C
C
get sample width

write(*,440)' Enter sample width : '
read(*,400) delr

C
C
C
open input data file

open(unit=38,file=infilnam,status='OLD')

C
C
C
open output file

open(unit=39,file=outfilnam,status='NEW')

C
C
C
read in the contour line values and echo to screen

do 100 i=1,nsamp,1          ! set up the row counter
do 110 j=1,nsamp,1          ! set up the col counter
read(38,err=1000,fmt=480) high ! highest contour line
read(38,err=1000,fmt=480) low  ! lowest contour line
zeta(i,j)=((high-low)/2.0)+low ! find mu(i,j) and save

```

```

        sigma(i,j)=(high-low)/4.0          ! find sigma(i,j) and save
C      write(*,400) zeta(i,j)
C      write(*,400) sigma(i,j)
        110 continue
        100 continue

C
C      calculate the mean estimate
C
        mu=0.0
        do 120 i=1,nsamp,1
        do 130 j=1,nsamp,1
        mu=mu+zeta(i,j)
        130 continue
        120 continue
        mu=mu/(nsamp**2)
        write(39,410) 'mu = ',mu
        write(*,410) 'mu = ',mu

C
C      calculate the height variance estimate
C
        hsqrd=0.0
        do 140 i=1,nsamp,1
        do 150 j=1,nsamp,1
        hsqrd=hsqrd+(zeta(i,j)-mu)**2
        150 continue
        140 continue
        hsqrd=hsqrd/(nsamp**2)
        write(39,420) 'hsqrd = ',hsqrd

```

```

write(*,420) 'hsqrd = ',hsqrd

C
C calculate the correlation length estimate
C

lsqrd=0.0
do 160 i=1,nsamp,1
do 170 j=1,nsamp,1
treg=0.0
do 180 m=1,nsamp,1
do 190 n=1,nsamp,1
rsqrd=((i-m)*delr)**2+((j-n)*delr)**2
logarg=(hsqrd-zeta(i,j)*zeta(m,n))
logarg=ABS(logarg/(sigma(i,j)*sigma(m,n)))
treg=rsqrd/LOG(logarg)
190 continue
180 continue
lsqrd=lsqrd+treg/(nsamp**2)
170 continue
160 continue
lsqrd=lsqrd/(nsamp**2)
write(39,420) 'lsqrd = ',lsqrd

C
C Save the sample means
C

do 200 i=1,nsamp,1
do 210 j=1,nsamp,1
write(39,490) 'mu('i','j') = ',zeta(i,j)
210 continue

```

200 continue

C

Save the sample standard deviations

C

C

do 220 i=1,nsamp,1

do 230 j=1,nsamp,1

write(39,500) 'sigma('i','j') = 'sigma(i,j)

230 continue

220 continue

goto 999

C

list of format statements

C

C

400 format(F8.3)

410 format(A6,F8.3)

420 format(A10,F8.3)

430 format(A25)

440 format(A35)

450 format(A15)

460 format(I4)

470 format(A10,F15.3)

480 format(F3.0)

490 format(A3,I2,A1,I2,A4,F8.3)

500 format(A6,I2,A1,I2,A4,F8.3)

C

detected error actions

C

C

1000 write(*,430)'!!! DATA READ ERROR !!!'

```

      goto 999
1010 write(*,430)'!!! DATA WRITE ERROR !!!'
C
C      close the data files and exit the program
C
      999 close(unit=38)
      close(unit=39)
      write(*,410) 'mu = ',mu
      write(*,420) 'hsqrd = ',hsqrd
      write(*,420) 'lsqrd = ',lsqrd
      stop
      end

```

The program implements Barrick's rough surface scattering formulas from the statistics of the characterization area generated with *Sitechar.for* and the transmitter, receiver, and target area geometry.

```

CCCCCCCCCCCCCCCCCCCCCCCCCCCCCCCCCCCCCCCCCCCCCCCCCCCCCCCCCCCC
C
C
C      SIGMA.FOR
C
C
C
CCCCCCCCCCCCCCCCCCCCCCCCCCCCCCCCCCCCCCCCCCCCCCCCCCCCCCCCCCCC
      IMPLICIT NONE
C
C      variable declarations

```

C

| | | |
|---------|-----------|------------------------|
| integer | i | ! loop index |
| integer | n | ! loop index |
| integer | m | ! loop index |
| complex | ctem | |
| real*8 | j | ! |
| real*8 | a1 | ! |
| real*8 | a2 | ! |
| real*8 | a3 | ! |
| real*8 | a4 | ! |
| real*8 | lsqrd | ! correlation length |
| real*8 | angi | ! |
| real*8 | treg | ! temp storage reg |
| real*8 | thetai | ! incident wave ang |
| real*8 | thetas | ! scattered wave an |
| real*8 | phis | ! scattered wave ph |
| real*8 | Dt | ! linear dist trans-cl |
| real*8 | Dr | ! linear dist rcvr-cl |
| real*8 | Db | ! linear dist trans-r |
| real*8 | ht | ! transmitter height |
| real*8 | hr | ! receiver height |
| real*8 | hc | ! clutter mean plan |
| real*8 | sigmavv | ! |
| real*8 | sigmahh | ! |
| complex | mur | ! relative permeabil |
| complex | epsilon_r | ! relative permittivi |
| complex | Rper | |
| complex | Rpar | |

| | | |
|--------------|-----------|-----------------------|
| real*8 | betavv | |
| real*8 | betahh | |
| real*8 | ssqrd | ! |
| real*8 | zetax | ! |
| real*8 | zetay | ! |
| real*8 | pi | |
| real*8 | cti | ! COS(thetai) |
| real*8 | sti | ! SIN(thetai) |
| real*8 | cts | ! COS(thetas) |
| real*8 | sts | ! SIN(thetas) |
| real*8 | cps | ! COS(phis) |
| real*8 | sps | ! SIN(phis) |
| complex | rooti | |
| real*8 | zetaz | |
| real*8 | si | ! SIN(angi) |
| real*8 | ci | ! COS(angi) |
| real*8 | nsamp | ! number of clutter |
| real*8 | beta | |
| real*8 | deltar | ! width of clut cell |
| real*8 | hsqrd | ! variance of clutter |
| character*15 | infilnam | ! file with height sa |
| character*15 | outfilnam | ! file with results |

C
C
C

initialize variables

| | |
|------------|-----------------------|
| ht=97.572 | ! set transmitter he |
| hr=144.0 | ! set receiver height |
| Db=19248.0 | ! set trans-rcvr dist |

| | |
|---|--|
| | pi=3.141592653589793 |
| C | |
| C | get input data file name |
| C | |
| | write(*,440)' Enter input data file name :' |
| | read(*,450) infilnam |
| C | |
| C | get output file name |
| C | |
| | write(*,440)' Enter output data file name:' |
| | read(*,450) outfilnam |
| C | |
| C | open input data file |
| C | |
| | open(unit=38,file=infilnam,status='OLD') |
| C | |
| C | open output file |
| C | |
| | open(unit=39,file=outfilnam,status='NEW') |
| C | |
| C | read in transmitter elevation and echo to screen |
| C | |
| | read(38,err=1000,fmt=400) Dt |
| | write(39,480)'Dt = ',Dt |
| | write(*,480)'Dt = ',Dt |
| C | |
| C | read in receiver elevation and echo to screen |
| C | |

```
read(38,err=1000,fmt=400) Dr
write(39,480)'Dr = ',Dr
write(*,480)'Dr = ',Dr
```

C

C

```
read in mean clutter height and echo to screen
```

C

```
read(38,err=1000,fmt=400) hc
write(39,480)'hc = ',hc
write(*,480)'hc = ',hc
```

C

C

```
read in relative permeability and echo to screen
```

C

```
read(38,err=1000,fmt=490) mur
write(39,500)'mu = ',mur
write(*,500)'mu = ',mur
```

C

C

```
read in relative permittivity and echo to screen
```

C

```
read(38,err=1000,fmt=490) epsilon_r
write(39,500)'eps = ',epsilon_r
write(*,500)'eps = ',epsilon_r
```

C

C

```
read in area of characterization site and echo to screen
```

C

```
read(38,err=1000,fmt=400) nsamp
write(39,480)'DIV = ',nsamp
write(*,480)'DIV = ',nsamp
read(38,err=1000,fmt=400) deltar
```

```

write(39,480)'DEL = ',deltar
write(*,480)'DEL = ',deltar

C
C
C
read in clutter variance and echo to screen

read(38,err=1000,fmt=400) hsqrd
write(39,480)'hsqrd = ',hsqrd
write(*,480)'hsqrd = ',hsqrd

C
C
C
read in correlation distance and echo to screen

read(38,err=1000,fmt=400) lsqrd
write(39,470)'lsqrd = ',lsqrd
write(*,470)'lsqrd = ',lsqrd

C
C
C
calculate the scattering angles

thetai=(pi/2.0)-DATAN((ht-hc)/Dt)
thetas=(pi/2.0)-DATAN((hr-hc)/Dr)
beta=DACOS((Dt**2+Dr**2-Db**2)/(2.0*Dt*Dr))
phis=pi-beta
write(39,470) 'tl tai = ',thetai
write(39,470) 'thetas = ',thetas
write(39,470) 'beta = ',beta
write(39,470) 'phis = ',phis
write(*,470) 'thetai = ',thetai
write(*,470) 'thetas = ',thetas
write(*,470) 'beta = ',beta

```

```

C      write(*,470) 'phis = ',phis
C
C      determine the angle i
C
      treg=1.0-DSIN(thetai)*DSIN(thetas)*DCOS(phis)
      treg=(treg+DCOS(thetai)*DCOS(thetas))/2.0
      angi=DACOS(DSQRT(treg))
      write(*,470) 'angle i = ',angi
      write(39,470) 'angle i = ',angi

```

```

C
C      determine the a coefficients
C

```

```

      cti=DCOS(thetai)
      sti=DSIN(thetai)
      cts=DCOS(thetas)
      sts=DSIN(thetas)
      cps=DCOS(phis)
      sps=DSIN(phis)
      a1=1.0+sti*sts*cps-cti*cts
      a2=cti*sts+sti*cts*cps
      a3=sti*cts+cti*sts*cps
      a4=cti+cts

```

```

C
C      determine the reflection coefficients
C

```

```

      ci=DCOS(angi)
      si=DSIN(angi)
      ctemp=(1.0,0.0)*si

```

```

rooti=CSQRT(mur*epsilon-(ctemp**2))
rper=(mur*ci-rooti)/(mur*ci+rooti)
rpar=(epsilon+ci-rooti)/(epsilon+ci+rooti)

C
C
C
determine zeta x,y, and z

zetax=sti-sts*cps
zetay=sts*sps
zetaz=0.0-cti-cps

C
C
C
determine s**2

ssqrd=4.0*hsqrd/lrqrd
write(39,470)'ssqrd = ',ssqrd
write(*,470)'ssqrd = ',ssqrd

C
C
C
determine J

j=(DEXP(0.0-(zetax**2+zetay**2)/(ssqrd*zetaz**2)))
j=j*4.0/(ssqrd*zetaz**2)
write(39,480)'j = 'j
write(*,480)'j = 'j

C
C
C
determine the scattering matrix components

ctemp=(a2+a3*rpar+sti*sts*(sps**2)*rper)/(a1+a4)
betavv=CABS(ctemp)
ctemp=(0.0-sti*sts*(sps**2)*rpar-a2+a3*rper)/(a1+a4)

```

betahh=CABS(ctemp)
write(39,470)'betavv = ',betavv
write(*,470)'betavv = ',betavv
write(39,470)'betahh = ',betahh
write(*,470)'betahh = ',betahh

C
C
C
C

determine the NRCS

sigmavv=(betavv**2)*j
sigmahh=(betahh**2)*j
write(39,470)'sigmavv = ',sigmavv
write(*,470)'sigmavv = ',sigmavv
write(39,470)'sigmahh = ',sigmahh
write(*,470)'sigmahh = ',sigmahh

C
C
C

list of format statements

400 format(F10.3)
410 format(A6,F10.3)
420 format(A10,F10.3)
430 format(A25)
440 format(A30)
450 format(A15)
460 format(I3)
470 format(' ',A10,E13.7)
480 format(' ',A9,E13.7)
490 format(F10.5,F10.5)

```

C      500 format(A9,F12.7,F12.7)
C
C      detected error actions
C
C      1000 write(*,430)'!!! DATA READ ERROR !!!'
C      1010 write(*,430)'!!! DATA WRITE ERROR !!!'
C
C      close the data files and exit the program
C
C      999 close(unit=38)
C      close(unit=39)
C      stop
C      end

```

Appendix B. *Topographic Data*

The data which follows is the site one contour line information used to estimate the site characterization area statistics.

[illegible]

| | y=1 | y=2 | y=3 | y=4 | y=5 |
|------|-------|-------|-------|-------|-------|
| x=1 | 60 57 | 60 57 | 60 57 | 63 57 | 63 57 |
| x=2 | 60 57 | 60 57 | 63 57 | 63 57 | 63 57 |
| x=3 | 63 60 | 63 60 | 69 60 | 69 60 | 69 60 |
| x=4 | 66 60 | 66 60 | 66 63 | 66 63 | 72 63 |
| x=5 | 66 60 | 66 63 | 69 63 | 69 63 | 69 66 |
| x=6 | 66 63 | 66 63 | 69 63 | 66 66 | 72 66 |
| x=7 | 66 63 | 69 63 | 69 66 | 72 66 | 75 69 |
| x=8 | 69 60 | 72 66 | 72 66 | 75 69 | 75 69 |
| x=9 | 72 66 | 75 69 | 78 69 | 78 72 | 81 72 |
| x=10 | 75 69 | 78 72 | 81 75 | 84 75 | 84 78 |
| x=11 | 75 69 | 81 75 | 84 78 | 84 81 | 87 81 |
| x=12 | 75 72 | 81 75 | 84 78 | 87 81 | 90 84 |
| x=13 | 75 72 | 81 75 | 84 78 | 90 81 | 93 84 |
| x=14 | 75 72 | 81 75 | 84 81 | 90 81 | 96 87 |
| x=15 | 78 72 | 84 75 | 87 81 | 93 84 | 96 90 |
| x=16 | 78 72 | 84 78 | 90 81 | 93 87 | 96 90 |
| x=17 | 81 75 | 84 81 | 90 84 | 93 87 | 96 90 |
| x=18 | 81 75 | 84 78 | 87 81 | 90 84 | 93 87 |
| x=19 | 81 75 | 84 78 | 84 81 | 87 81 | 87 81 |
| x=20 | 78 72 | 81 75 | 81 75 | 81 75 | 81 75 |

| | y=6 | y=7 | y=8 | y=9 | y=10 |
|------|--------|---------|---------|---------|---------|
| x=1 | 63 60 | 63 60 | 66 60 | 66 63 | 66 63 |
| x=2 | 63 60 | 66 60 | 66 63 | 69 63 | 69 66 |
| x=3 | 69 60 | 72 63 | 72 63 | 72 66 | 72 66 |
| x=4 | 72 63 | 69 66 | 69 66 | 72 63 | 72 69 |
| x=5 | 72 66 | 72 66 | 72 66 | 75 66 | 75 69 |
| x=6 | 72 69 | 75 69 | 75 69 | 75 72 | 78 72 |
| x=7 | 75 69 | 75 69 | 78 69 | 78 72 | 81 75 |
| x=8 | 75 69 | 78 72 | 78 72 | 78 75 | 81 75 |
| x=9 | 81 75 | 81 75 | 84 75 | 87 78 | 90 78 |
| x=10 | 84 78 | 87 78 | 90 81 | 93 84 | 102 87 |
| x=11 | 90 81 | 93 84 | 96 87 | 102 90 | 105 93 |
| x=12 | 93 84 | 99 90 | 102 90 | 108 99 | 111 102 |
| x=13 | 99 90 | 105 93 | 108 99 | 111 105 | 114 108 |
| x=14 | 102 90 | 105 99 | 111 102 | 114 108 | 114 111 |
| x=15 | 105 96 | 108 102 | 111 105 | 111 105 | 111 105 |
| x=16 | 102 96 | 105 99 | 111 102 | 105 99 | 105 99 |
| x=17 | 102 93 | 102 93 | 102 90 | 102 90 | 99 87 |
| x=18 | 96 87 | 96 87 | 93 84 | 90 81 | 90 78 |
| x=19 | 87 81 | 87 78 | 84 78 | 84 75 | 81 75 |
| x=20 | 81 75 | 81 72 | 78 72 | 78 75 | 81 75 |

| | y=11 | y=12 | y=13 | y=14 | y=15 |
|------|---------|---------|---------|---------|---------|
| x=1 | 66 63 | 66 63 | 66 63 | 66 63 | 66 63 |
| x=2 | 69 63 | 69 63 | 69 63 | 72 63 | 72 63 |
| x=3 | 72 66 | 69 66 | 72 66 | 72 69 | 72 69 |
| x=4 | 75 69 | 75 69 | 78 69 | 78 72 | 78 72 |
| x=5 | 75 72 | 78 72 | 78 72 | 78 75 | 78 75 |
| x=6 | 81 72 | 81 75 | 81 75 | 84 75 | 84 75 |
| x=7 | 84 75 | 87 78 | 87 81 | 90 81 | 90 84 |
| x=8 | 84 75 | 90 78 | 93 81 | 96 84 | 96 87 |
| x=9 | 96 84 | 102 90 | 102 90 | 102 93 | 102 96 |
| x=10 | 105 90 | 105 99 | 108 99 | 108 99 | 108 102 |
| x=11 | 108 102 | 111 105 | 111 105 | 111 105 | 108 105 |
| x=12 | 114 105 | 114 108 | 114 108 | 111 108 | 111 105 |
| x=13 | 114 111 | 114 111 | 114 108 | 111 105 | 108 102 |
| x=14 | 114 111 | 114 108 | 114 111 | 114 108 | 114 108 |
| x=15 | 111 102 | 111 105 | 111 102 | 108 96 | 102 87 |
| x=16 | 105 96 | 105 93 | 102 90 | 96 87 | 93 84 |
| x=17 | 96 84 | 96 84 | 93 84 | 90 84 | 87 81 |
| x=18 | 87 81 | 87 81 | 87 81 | 84 78 | 84 81 |
| x=19 | 84 81 | 84 81 | 84 81 | 84 78 | 84 78 |
| x=20 | 84 78 | 81 78 | 84 75 | 81 75 | 81 75 |

cc

| | y=16 | y=17 | y=18 | y=19 | y=20 |
|------|---------|--------|-------|-------|-------|
| x=1 | 66 63 | 66 63 | 66 63 | 66 63 | 66 63 |
| x=2 | 69 63 | 69 63 | 66 63 | 69 63 | 69 63 |
| x=3 | 72 66 | 72 66 | 69 63 | 69 66 | 69 66 |
| x=4 | 78 69 | 75 69 | 75 66 | 72 66 | 72 66 |
| x=5 | 78 75 | 81 72 | 81 69 | 75 69 | 75 69 |
| x=6 | 84 75 | 84 78 | 84 78 | 81 75 | 81 72 |
| x=7 | 87 81 | 87 81 | 90 81 | 87 78 | 84 73 |
| x=8 | 99 87 | 99 87 | 96 87 | 93 84 | 87 81 |
| x=9 | 102 96 | 99 96 | 99 90 | 96 87 | 90 84 |
| x=10 | 105 99 | 102 96 | 99 93 | 96 87 | 90 81 |
| x=11 | 105 102 | 102 99 | 99 93 | 93 87 | 87 81 |
| x=12 | 105 99 | 102 96 | 99 90 | 93 84 | 87 81 |
| x=13 | 105 99 | 99 93 | 96 87 | 90 84 | 87 81 |
| x=14 | 108 102 | 102 90 | 93 81 | 87 81 | 84 78 |
| x=15 | 96 84 | 90 81 | 87 81 | 84 78 | 81 72 |
| x=16 | 90 81 | 84 81 | 84 78 | 81 78 | 81 75 |
| x=17 | 84 81 | 84 81 | 84 78 | 81 75 | 78 72 |
| x=18 | 84 78 | 84 78 | 81 75 | 78 72 | 75 72 |
| x=19 | 81 75 | 78 72 | 78 72 | 75 72 | 75 69 |
| x=20 | 81 75 | 75 72 | 75 69 | 75 69 | 75 66 |

[illegible]

| | y=1 | y=2 | y=3 | y=4 | y=5 |
|------|---------|---------|---------|--------|--------|
| x=1 | 87 69 | 90 78 | 93 81 | 93 84 | 93 84 |
| x=2 | 93 78 | 96 87 | 96 90 | 96 90 | 96 90 |
| x=3 | 93 78 | 99 93 | 102 93 | 102 96 | 99 93 |
| x=4 | 99 87 | 102 96 | 102 99 | 102 96 | 99 96 |
| x=5 | 105 96 | 105 99 | 105 99 | 102 99 | 99 96 |
| x=6 | 105 99 | 105 102 | 105 99 | 102 99 | 99 96 |
| x=7 | 108 102 | 103 102 | 105 102 | 105 99 | 102 96 |
| x=8 | 108 102 | 103 102 | 105 102 | 105 99 | 102 96 |
| x=9 | 108 99 | 108 102 | 105 99 | 102 96 | 102 93 |
| x=10 | 102 90 | 102 96 | 102 96 | 102 93 | 99 90 |
| x=11 | 96 87 | 99 93 | 99 93 | 99 90 | 96 87 |
| x=12 | 93 81 | 96 90 | 96 90 | 96 87 | 90 81 |
| x=13 | 90 81 | 93 87 | 93 84 | 90 81 | 87 78 |
| x=14 | 90 78 | 90 78 | 90 75 | 84 72 | 81 72 |
| x=15 | 78 72 | 78 72 | 78 69 | 75 69 | 75 69 |
| x=16 | 72 63 | 72 63 | 72 66 | 72 66 | 72 63 |
| x=17 | 69 60 | 66 60 | 66 60 | 66 60 | 66 60 |
| x=18 | 63 60 | 63 60 | 63 57 | 63 57 | 63 57 |
| x=19 | 60 54 | 60 54 | 60 57 | 63 60 | 60 57 |
| x=20 | 60 57 | 60 57 | 63 57 | 63 60 | 63 60 |

[illegible]

| | y=6 | y=7 | y=8 | y=9 | y=10 |
|------|-------|-------|-------|-------|-------|
| x=1 | 90 81 | 87 78 | 84 75 | 84 75 | 81 72 |
| x=2 | 93 87 | 93 84 | 90 81 | 87 78 | 84 78 |
| x=3 | 96 90 | 96 90 | 93 87 | 90 84 | 90 81 |
| x=4 | 99 93 | 96 93 | 96 90 | 93 87 | 90 87 |
| x=5 | 99 93 | 96 93 | 96 90 | 93 90 | 90 87 |
| x=6 | 99 93 | 96 93 | 96 93 | 93 90 | 93 87 |
| x=7 | 99 96 | 99 93 | 96 93 | 93 90 | 93 87 |
| x=8 | 99 96 | 99 93 | 96 90 | 93 87 | 90 84 |
| x=9 | 99 90 | 96 90 | 93 87 | 90 84 | 87 81 |
| x=10 | 96 87 | 93 84 | 90 81 | 87 81 | 84 78 |
| x=11 | 90 81 | 87 81 | 84 78 | 84 75 | 81 75 |
| x=12 | 87 81 | 84 78 | 81 75 | 81 75 | 78 72 |
| x=13 | 84 75 | 81 72 | 78 69 | 78 69 | 75 69 |
| x=14 | 78 69 | 75 69 | 72 66 | 69 60 | 69 60 |
| x=15 | 72 66 | 72 66 | 69 63 | 66 63 | 66 60 |
| x=16 | 69 63 | 69 63 | 66 60 | 66 60 | 63 60 |
| x=17 | 66 60 | 66 60 | 63 60 | 63 57 | 63 57 |
| x=18 | 63 57 | 63 57 | 63 57 | 60 57 | 60 57 |
| x=19 | 60 57 | 60 57 | 60 57 | 60 57 | 60 57 |
| x=20 | 63 60 | 63 60 | 60 57 | 60 57 | 60 57 |

ccccccccc:cc

| | y=11 | y=12 | y=13 | y=14 | y=15 |
|------|-------|-------|-------|-------|-------|
| x=1 | 78 69 | 75 69 | 75 69 | 75 69 | 72 66 |
| x=2 | 81 75 | 81 75 | 81 75 | 78 72 | 75 69 |
| x=3 | 87 81 | 84 78 | 81 78 | 78 72 | 75 69 |
| x=4 | 90 84 | 84 78 | 84 78 | 78 75 | 75 69 |
| x=5 | 90 84 | 87 81 | 84 76 | 78 75 | 75 69 |
| x=6 | 90 84 | 87 81 | 84 78 | 78 72 | 75 66 |
| x=7 | 90 84 | 84 75 | 84 75 | 78 69 | 72 66 |
| x=8 | 84 78 | 81 78 | 78 72 | 75 66 | 69 63 |
| x=9 | 84 78 | 81 75 | 78 69 | 75 66 | 69 63 |
| x=10 | 81 75 | 78 72 | 75 69 | 72 66 | 69 66 |
| x=11 | 78 75 | 78 72 | 75 69 | 75 66 | 72 69 |
| x=12 | 78 69 | 75 69 | 72 66 | 69 66 | 69 66 |
| x=13 | 75 66 | 72 66 | 69 63 | 69 63 | 69 63 |
| x=14 | 69 63 | 69 63 | 66 60 | 66 60 | 66 60 |
| x=15 | 66 60 | 66 60 | 63 60 | 63 60 | 63 60 |
| x=16 | 63 57 | 63 57 | 63 57 | 63 57 | 63 57 |
| x=17 | 60 57 | 60 57 | 60 57 | 60 57 | 60 57 |
| x=18 | 60 57 | 60 57 | 60 54 | 60 54 | 60 54 |
| x=19 | 60 54 | 57 54 | 57 54 | 60 54 | 60 57 |
| x=20 | 60 54 | 60 54 | 60 54 | 60 57 | 60 57 |

| | y=16 | y=17 | y=18 | y=19 | y=20 |
|------|-------|-------|-------|-------|-------|
| x=1 | 69 63 | 66 63 | 63 60 | 63 57 | 60 57 |
| x=2 | 69 63 | 66 63 | 63 60 | 60 57 | 60 57 |
| x=3 | 69 66 | 66 63 | 63 60 | 60 57 | 57 54 |
| x=4 | 69 66 | 66 63 | 63 60 | 63 57 | 60 54 |
| x=5 | 69 66 | 66 60 | 63 60 | 63 60 | 60 57 |
| x=6 | 69 63 | 66 60 | 63 60 | 63 60 | 60 57 |
| x=7 | 69 63 | 63 60 | 63 60 | 63 60 | 60 57 |
| x=8 | 66 60 | 63 60 | 63 60 | 63 57 | 60 57 |
| x=9 | 66 60 | 69 60 | 66 60 | 66 60 | 63 57 |
| x=10 | 69 66 | 69 66 | 69 63 | 66 60 | 63 60 |
| x=11 | 72 69 | 72 66 | 69 63 | 66 60 | 63 60 |
| x=12 | 72 66 | 72 66 | 69 63 | 66 60 | 63 60 |
| x=13 | 69 63 | 69 63 | 66 60 | 63 60 | 63 60 |
| x=14 | 66 60 | 66 60 | 63 60 | 63 57 | 63 57 |
| x=15 | 63 60 | 63 60 | 63 57 | 63 57 | 60 54 |
| x=16 | 60 57 | 63 57 | 63 57 | 60 57 | 60 54 |
| x=17 | 60 57 | 60 57 | 60 57 | 60 57 | 60 54 |
| x=18 | 60 57 | 60 57 | 60 57 | 60 57 | 60 54 |
| x=19 | 60 57 | 60 57 | 60 57 | 60 57 | 57 54 |
| x=20 | 60 54 | 60 54 | 60 54 | 60 51 | 57 51 |

CC

B-9

| | y=6 | y=7 | y=8 | y=9 | y=10 |
|------|-------|-------|-------|-------|-------|
| x=1 | 42 36 | 42 36 | 39 36 | 39 36 | 39 36 |
| x=2 | 39 36 | 39 36 | 39 36 | 39 36 | 39 36 |
| x=3 | 39 36 | 39 36 | 39 36 | 39 36 | 39 36 |
| x=4 | 39 36 | 39 36 | 39 36 | 39 36 | 39 36 |
| x=5 | 39 36 | 39 36 | 39 36 | 39 36 | 39 36 |
| x=6 | 39 36 | 39 36 | 39 36 | 39 36 | 39 36 |
| x=7 | 42 39 | 42 39 | 42 36 | 42 36 | 42 39 |
| x=8 | 45 39 | 45 39 | 45 39 | 45 39 | 45 39 |
| x=9 | 54 45 | 54 45 | 51 42 | 51 42 | 48 42 |
| x=10 | 60 51 | 57 51 | 57 48 | 57 48 | 54 42 |
| x=11 | 63 57 | 66 57 | 63 57 | 63 54 | 60 48 |
| x=12 | 66 63 | 66 63 | 69 63 | 69 60 | 66 54 |
| x=13 | 69 63 | 69 63 | 72 66 | 72 66 | 69 60 |
| x=14 | 69 63 | 69 63 | 72 63 | 72 66 | 72 63 |
| x=15 | 66 60 | 66 60 | 66 63 | 69 63 | 69 60 |
| x=16 | 63 54 | 66 54 | 66 57 | 66 57 | 66 57 |
| x=17 | 54 48 | 60 48 | 63 48 | 60 51 | 60 51 |
| x=18 | 51 45 | 51 45 | 51 45 | 51 45 | 54 45 |
| x=19 | 48 39 | 48 42 | 48 42 | 48 42 | 48 42 |
| x=20 | 42 39 | 45 39 | 45 39 | 45 39 | 45 39 |

cc

| | y=11 | y=12 | y=13 | y=14 | y=15 |
|------|-------|-------|-------|-------|-------|
| x=1 | 39 36 | 39 36 | 39 36 | 39 36 | 39 36 |
| x=2 | 39 36 | 39 36 | 39 36 | 39 36 | 39 36 |
| x=3 | 39 36 | 39 36 | 39 36 | 39 36 | 39 36 |
| x=4 | 39 36 | 39 36 | 39 36 | 39 36 | 39 36 |
| x=5 | 39 36 | 39 36 | 39 36 | 39 36 | 39 36 |
| x=6 | 39 36 | 39 36 | 39 36 | 39 36 | 39 36 |
| x=7 | 42 39 | 42 39 | 42 39 | 42 39 | 42 36 |
| x=8 | 42 39 | 42 39 | 42 39 | 42 39 | 42 39 |
| x=9 | 45 39 | 45 39 | 42 39 | 42 39 | 42 39 |
| x=10 | 48 39 | 45 39 | 42 39 | 42 39 | 42 39 |
| x=11 | 57 45 | 51 39 | 45 39 | 42 39 | 42 39 |
| x=12 | 63 48 | 57 45 | 51 39 | 45 39 | 42 39 |
| x=13 | 66 54 | 60 48 | 51 42 | 48 39 | 45 39 |
| x=14 | 66 57 | 63 54 | 57 48 | 51 42 | 45 39 |
| x=15 | 66 57 | 63 54 | 57 45 | 48 42 | 45 39 |
| x=16 | 63 51 | 60 48 | 54 42 | 54 42 | 45 39 |
| x=17 | 57 48 | 54 45 | 48 42 | 45 39 | 42 39 |
| x=18 | 54 45 | 51 39 | 45 42 | 45 39 | 42 39 |
| x=19 | 48 39 | 45 39 | 45 39 | 42 39 | 42 39 |
| x=20 | 42 39 | 42 39 | 42 39 | 42 39 | 42 39 |

| | $y=16$ | $y=17$ | $y=18$ | $y=19$ | $y=20$ |
|--------|--------|--------|--------|--------|--------|
| $x=1$ | 39 36 | 39 36 | 39 36 | 39 36 | 39 36 |
| $x=2$ | 39 36 | 39 36 | 39 36 | 39 36 | 39 36 |
| $x=3$ | 39 36 | 39 36 | 39 36 | 39 36 | 39 36 |
| $x=4$ | 39 36 | 39 36 | 39 36 | 39 36 | 39 36 |
| $x=5$ | 39 36 | 39 36 | 39 36 | 45 36 | 45 36 |
| $x=6$ | 39 36 | 39 36 | 42 36 | 45 39 | 48 42 |
| $x=7$ | 42 36 | 39 36 | 42 36 | 45 39 | 45 42 |
| $x=8$ | 42 36 | 39 36 | 42 36 | 45 39 | 51 45 |
| $x=9$ | 42 39 | 39 36 | 42 36 | 45 39 | 51 45 |
| $x=10$ | 42 36 | 39 36 | 42 36 | 48 36 | 51 42 |
| $x=11$ | 42 36 | 39 36 | 39 36 | 45 36 | 48 39 |
| $x=12$ | 42 36 | 39 36 | 42 36 | 42 36 | 45 39 |
| $x=13$ | 42 36 | 39 36 | 39 36 | 39 36 | 42 36 |
| $x=14$ | 42 39 | 42 39 | 42 39 | 39 36 | 39 36 |
| $x=15$ | 42 39 | 42 39 | 42 39 | 42 39 | 39 36 |
| $x=16$ | 42 39 | 42 39 | 42 39 | 42 36 | 39 36 |
| $x=17$ | 42 39 | 42 39 | 42 39 | 42 36 | 39 36 |
| $x=18$ | 42 39 | 42 39 | 42 36 | 39 36 | 39 36 |
| $x=19$ | 42 39 | 42 39 | 42 36 | 39 36 | 39 36 |
| $x=20$ | 42 39 | 42 39 | 42 36 | 39 36 | 39 36 |

Bibliography

1. Balanis, Constantine A. *Advanced Electromagnetic Engineering*. New York: John Wiley and Sons, 1989.
2. Barksdale, Harry Class Notes from EENG 625 Antennas. School of Engineering, Air Force Institute of Technology (AU), Wright-Patterson AFB OH, 1990.
3. Beckmann, Petr and Andre Spizzichino. *The Scattering of Electromagnetic Waves From Rough Surfaces*. New York: Artech House, 1987.
4. Beyer, William H. *CRC Standard Mathematical Tables*. Boca Raton: CRC Press, 1987.
5. Brown, Gary S. *A Theoretical Study of the Effects of Vegetation on Terrain Scattering: Final Technical Report*. Rome Air Development Center, Griffiss AFB NY, March 1988
6. Fung, Adrian K. *Effect of Cell Size on Radar Clutter Statistics: Final Technical Report*. Rome Air Development Center, Griffiss AFB NY, September 1990
7. Kraus, John D. *Antennas*. New York NY: McGraw-Hill Book Company, 1950.
8. Lennon, John F. et al. *Bistatic Radar Clutter Cross Section for Large Bistatic Angles*. Rome Air Development Center In-House Report, RADC-TR-88-171, Jun 1988.
9. Long, Maurice W. *Radar Reflectivity of Land and Sea*. Lexington MA: Lexington Books, 1975.
10. Milligan, Thomas A. *Modern Antenna Design*. New York: McGraw-Hill Book Company, 1985.
11. Pozar, David M. *Microwave Engineering*. Reading MA: Addison-Wesley Publishing Company, 1990.
12. Roseman, Capt Thomas K. *Electromagnetic Scattering by an Exponentially Distributed Rough Surface with the Introduction of a Rough Surface Generation Technique*. MS Thesis, AFIT/GE/87D-55. School of Electrical Engineering, Air Force Institute of Technology (AU), Wright-Patterson AFB OH, Dec 1987.
13. Ruck, George T. et al. *Radar Cross Section Handbook*, Volume 2. New York: Plenum Press, 1970.
14. Skolnik, Merrill I. *Introduction to Radar Systems*. New York: McGraw-Hill, 1980.
15. Skolnik Merrill I. *Radar Handbook*. New York: McGraw-Hill, 1970.
16. SRS Technologies *Bistatic Clutter Phenomenologica/Model Development: Final Technical Report*. Rome Air Development Center, Griffiss AFB NY, May 1983.

17. Stutzman, Warren L. and Thiele, Gary A. *Antenna Theory and Design*. New York: John Wiley and Sons, 1981.
18. Willis, Nicholas J. *Bistatic Radar*. Norwood MA: Artech House, 1991

Vita

Captain Clyde R. Heddings was born on 30 July, 1953 in Milton, Pennsylvania. In 1971, he graduated from Coral Shores High School located in Tavernier, Florida. Captain Heddings was accepted in the Airman's Education and Commissioning Program in 1984 and received his Bachelor of Science in Engineering degree from Wright State University in 1986. Upon graduation he attended Officers Training School and earned a commission in the USAF. From there, he was assigned to the Information Transmission Branch, Systems Avionics Division, Avionics Laboratory where he remained until entering the School of Engineering, Air Force Institute of Technology, in May 1990.

Permanent address: 241 Hispanola Drive
Tavernier, Florida 33070

END

FILMED

DATE: 1-92

DTIC